



National Library
of Canada

Bibliothèque nationale
du Canada

Canadian Theses Service / Service des thèses canadiennes

Ottawa, Canada
K1A 0N4

NOTICE

The quality of this microform is heavily dependent upon the quality of the original thesis submitted for microfilming. Every effort has been made to ensure the highest quality of reproduction possible.

If pages are missing, contact the university which granted the degree.

Some pages may have indistinct print especially if the original pages were typed with a poor typewriter ribbon or if the university sent us an inferior photocopy.

Previously copyrighted materials (journal articles, published tests, etc.) are not filmed.

Reproduction in full or in part of this microform is governed by the Canadian Copyright Act, R.S.C. 1970, c. C-30.

AVIS

La qualité de cette microforme dépend grandement de la qualité de la thèse soumise au microfilmage. Nous avons tout fait pour assurer une qualité supérieure de reproduction.

S'il manque des pages, veuillez communiquer avec l'université qui a conféré le grade.

La qualité d'impression de certaines pages peut laisser à désirer, surtout si les pages originales ont été dactylographiées à l'aide d'un ruban usé ou si l'université nous a fait parvenir une photocopie de qualité inférieure.

Les documents qui font déjà l'objet d'un droit d'auteur (articles de revue, tests publiés, etc.) ne sont pas microfilmés.

La reproduction, même partielle, de cette microforme est soumise à la Loi canadienne sur le droit d'auteur, SRC 1970, c. C-30.

THE UNIVERSITY OF ALBERTA

Thermodynamic Investigations. 1. Thermodynamic Properties of Aqueous
Aluminum Ion 2. Kinetics and Energetics of Low Temperature Oxidation of
Athabasca Bitumen

BY

Leslie Barta

A THESIS

SUBMITTED TO THE FACULTY OF GRADUATE STUDIES AND RESEARCH
IN PARTIAL FULFILLMENT OF THE REQUIREMENTS FOR THE DEGREE
OF DOCTOR OF PHILOSOPHY

DEPARTMENT OF CHEMISTRY

EDMONTON, ALBERTA

FALL, 1987

Permission has been granted to the National Library of Canada to microfilm this thesis and to lend or sell copies of the film.

The author (copyright owner) has reserved other publication rights, and neither the thesis nor extensive extracts from it may be printed or otherwise reproduced without his/her written permission.

L'autorisation a été accordée à la Bibliothèque nationale du Canada de microfilmer cette thèse et de prêter ou de vendre des exemplaires du film.

L'auteur (titulaire du droit d'auteur) se réserve les autres droits de publication; ni la thèse ni de longs extraits de celle-ci ne doivent être imprimés ou autrement reproduits sans son autorisation écrite.

ISBN 0-315-41044-2

THE UNIVERSITY OF ALBERTA

RELEASE FORM

NAME OF AUTHOR: Leslie Barta

TITLE OF THESIS: Thermodynamic Investigations. 1. Thermodynamic Properties of Aqueous Aluminum Ion 2. Kinetics and Energetics of Low Temperature Oxidation of Athabasca Bitumen

DEGREE: Doctor of Philosophy

YEAR THIS DEGREE GRANTED: 1987

Permission is hereby granted to THE UNIVERSITY OF ALBERTA LIBRARY to reproduce single copies of this thesis and to lend or sell such copies for private, scholarly or scientific research purposes only.

The author reserves other publication rights, and neither the thesis nor extensive extracts from it may be printed or otherwise reproduced without the author's written permission.

Leslie Barta

950 Locust St.

Butte, Montana 59701

USA

Date: May 26, 1987

THE UNIVERSITY OF ALBERTA
FACULTY OF GRADUATE STUDIES AND RESEARCH

The undersigned certify that they have read, and recommend to the Faculty of Graduate Studies and Research, for acceptance, a thesis entitled **Thermodynamic Investigations. 1. Thermodynamic Properties of Aqueous Aluminum Ion 2. Kinetics and Energetics of Low Temperature Oxidation of Athabasca Bitumen** submitted by Leslie A. Barta in partial fulfillment of the requirements for the degree of DOCTOR OF PHILOSOPHY.

Loren E. Hyatt

Supervisor

Thomas Zentgraf

James A. Plank

Serge Kotoch

Earl M. Woolley

External Examiner

Date May 26, 1987

Abstract

Densities of aqueous solutions of AlCl_3 (containing dilute HCl) have been measured at 10, 25, 40, and 55°C with results that have led to apparent molar volumes. The Pitzer ion interaction model has been used for analyzing these apparent molar volumes to obtain corresponding standard state partial molar volumes of $\text{AlCl}_3(\text{aq})$. Similar use has been made of published apparent molar heat capacities of aqueous solutions of $\text{AlCl}_3\text{-HCl}$ and $\text{Al}(\text{NO}_3)_3\text{-HNO}_3$ to obtain standard state partial molar heat capacities of $\text{AlCl}_3(\text{aq})$ and $\text{Al}(\text{NO}_3)_3(\text{aq})$. The partial molar volumes and heat capacities have been used with the Helgeson-Kirkham semi-theoretical equation of state for aqueous ions to provide a basis for estimating the thermodynamic properties of $\text{Al}^{3+}(\text{aq})$ at high temperatures and pressures. This work presents improved volumetric data for $\text{Al}^{3+}(\text{aq})$, a phenomenologically consistent treatment of volumetric and thermal properties of a solution of mixed aqueous electrolytes containing a trivalent cation, and the first semi-theoretical representation of the temperature dependence of the standard state volume and heat capacity of a trivalent cation.

An aneroid calorimeter has been designed and built for measuring rates of oxidation of bitumen in porous medium under nearly isothermal conditions in the temperature range 155-320°C and in flowing gas atmosphere at pressures

to 400 kPa absolute. Rates measured at 155 and 210°C at several pressures of oxygen have been used to assess the performance of the calorimeter and to define the limitations of this method. A general method of analysis of thermokinetic data for slow exothermic reactions has been developed.

Application of a factorial experimental design to measurements of the rate of oxidation of Athabasca bitumen has led to the identification of two classes of reactions occurring in this temperature range, with the "transition" temperature near 285°C. This result has been supported by chemical analyses and energy relationships. The combined results indicate that oxidation of bitumen at low temperatures proceeds by way of oxidative pyrolysis of the asphaltene fraction with simultaneous distillation of the saturate and aromatic fractions. At high temperatures complete combustion occurs. Apparent activation energies, reaction orders for oxygen, and pre-exponential factors for both processes have been evaluated.

Acknowledgements

In connection with the first part of this research I thank P. R. Tremaine and the Alberta Research Council for allowing me to use their densimeter. I would also like to thank J. K. Hovey and P. R. Tremaine for giving me the results of their measurements of heat capacities before publication and for helpful discussions.

In connection with the second part of this research I am most grateful to Z.-L. Zhang, who provided the results of his kinetic measurements at 210°C and much good advice. Sincere appreciation is extended to Y.-M. Xu, who prepared one of the calorimetric samples, to D. D. McIntyre, who performed the chromatographic separations and GC analyses, and to J. F. Smith, whose helpful discussions have been invaluable. I also thank the personnel in the electronics and machine shops, microanalytical laboratory, and spectral services for their contributions.

In all aspects of this research I am especially grateful to my research advisor, Loren G. Hepler, for providing opportunity, freedom of inquiry, and generous funding. We thank the Natural Sciences and Engineering Research Council of Canada and the Alberta Oil Sands Technology and Research Authority for their support of this research.

I especially thank my husband, Steve McGrath, for his help and encouragement.

Table of Contents

	Page
Abstract	iv
Acknowledgements	vi
List of Tables	ix
List of Figures	xi
Introduction	1
<u>Chapter</u>	
1. Densities and Apparent Molar Volumes of Aqueous Aluminum Chloride. Analysis of Apparent Molar Volumes and Heat Capacities of Aqueous Aluminum Salts in terms of the Pitzer and Helgeson Theoretical Models	2
Introduction	2
Experimental	4
Results and Calculations	5
Discussion	21
2. Construction and Testing of an Aneroid Calorimeter for Investigating the Rates of Slow Reactions, with Application to the Low Temperature Oxidation of Athabasca Bitumen	28
Introduction	28
Experimental	32

Table of Contents (continued)

<u>Chapter</u>	Page
Materials	32
Operation	33
Interpretation of Data	35
Calibration	35
Oxidation of Bitumen	42
Results	46
3. Kinetics and Energetics of Oxidation of Athabasca Bitumen	55
Introduction	55
Experimental	56
Design of Experiments	57
Results and Calculations	59
Initial Rates of Heat Production	59
Formation of Coke	72
Analysis of Cokes and Distillates	79
Discussion	84
References	92
Appendix A	98
Appendix B	102

List of Tables

Table	Page
1-1. Compositions and densities of aqueous mixtures of aluminum chloride and hydrochloric acid	7
1-2. Smoothed Pitzer interaction model parameters for apparent molar volumes of HCl estimated from the fit to data from Akerlof and Teare	12
1-3. Standard partial molar volume of aqueous AlCl_3 obtained by extrapolation using the Pitzer interaction model	12
1-4. Coefficients for apparent molar volume of AlCl_3	13
1-5. Smoothed Pitzer interaction model parameters for apparent molar heat capacities of HCl calculated from the equations given by Tremaine, Sway, and Barbero	17
1-6. Coefficients for apparent molar heat capacity of AlCl_3	17
1-7. Standard partial molar heat capacity of $\text{AlCl}_3(\text{aq})$ obtained by extrapolation using the Pitzer interaction model	19
1-8. Coefficients for the Helgeson-Kirkham model for the standard state partial molar properties of $\text{Al}^{3+}(\text{aq})$	19
1-9. Pitzer interaction model parameters for apparent molar volumes and heat capacities of HNO_3 and $\text{Al}(\text{NO}_3)_3$ at 25°C	27
2-1. Rates of production of heat during oxidation of Athabasca bitumen at 155 and 210°C	47
2-2. Calibration constants for 155 and 210°C	48
2-3. Kinetic parameters for the low temperature oxidation of Athabasca bitumen	48
3-1. Initial rates of heat production during slow oxidation of bitumen, first order factorial design	60

List of Tables (continued)

Table	Page
3-2. Comparison of kinetic parameters derived from first order response surface measurements with those derived from sets of isothermal measurements at 155 and 210°C using the Arrhenius equation	61
3-3. Analysis of variance for a first order factorial design model	61
3-4. Initial rate of heat production during slow oxidation of bitumen, second order factorial design	63
3-5. Analysis of variance for a full second order factorial design model	64
3-6. Analysis of variance for a partial second order factorial design model	66
3-7. Model parameters for initial rate of heat production during low temperature oxidation of bitumen	67
3-8. Initial rates of heat production for use in isothermal evaluation of kinetic parameters	67
3-9. Coefficients for initial rate of heat production, rate constant, and reaction order with respect to oxygen	70
3-10. Total heat produced during slow oxidation of bitumen	73
3-11. Coke deposited and burned during slow oxidation of bitumen	77
3-12. Parameters for total heat produced	78
3-13. Parameters for deposition of coke	78
3-14. Elemental compositions of tar sands and their constituents before and after low temperature oxidation at 210 kPa O ₂	80
3-15. Tar sand distillates collected at room temperature during slow oxidation of bitumen	83
3-16. Fractionation of original bitumen and produced oil	83

List of Figures

Figure	Page
1-1. Temperature dependence of binary interaction parameters for the apparent molar volumes of aluminum chloride from 10-55°C	14
1-2. Temperature dependence of binary interaction parameter for the apparent molar heat capacity of aluminum chloride from 10-55°C	18
1-3. Temperature dependence of the standard partial molar (a) volume and (b) heat capacity of $\text{Al}^{3+}(\text{aq})$	22
1-4. Apparent molar volume of aluminum chloride from 10-55°C, corrected for the Debye-Huckel electrostatic contribution	23
1-5. Apparent molar heat capacity of aluminum chloride from 10-55°C, corrected for the Debye-Huckel electrostatic contribution	24
2-1. Partial section of the aneroid calorimeter	33
2-2. Schematic diagram of the calorimetric apparatus for measuring the rate of oxidation of bitumen at low temperatures	36
2-3. Reconstruction of calorimetric records by calibration with electrical energy: (a) time-dependence of power input and power response corrected for thermal lags and heat losses (b) time-dependence of temperature rise	38
2-4. Time-dependence of total energy input and energy response corrected for thermal lags and heat losses during calibration	43
2-5. Time-dependence of (a) power development and (b) energy release during LTO of bitumen at 210°C and 125 kPa O_2	44
3-1. Temperature dependence of the global rate constant for oxidation of Athabasca bitumen at low temperatures	71
3-2. Temperature dependence of the reaction order with respect to oxygen for the global oxidation of Athabasca bitumen at low temperatures	71
3-3. Effect of oxygen partial pressure on the time of completion of depositional reactions during LTO of Athabasca bitumen	91

Introduction

The work presented here consists of two separate investigations in the field of experimental thermochemistry, one concerned with the equilibrium chemistry of aqueous solutions of electrolytes and one concerned with the kinetics of slow reactions involving a solid and a gas phase. Chapter 1 treats the first topic, the thermodynamic properties of aqueous aluminum ion. Chapters 2 and 3 treat the second topic, the rate of reaction of bitumen with oxygen at low temperatures. The calorimetric apparatus and method of investigating oxidation kinetics are presented in Chapter 2. Application of the apparatus and method to the development of a kinetic model for the oxidation of bitumen at low temperatures is presented in Chapter 3.

The oxidation kinetics of bitumen at low temperatures is primarily of interest in connection with the *in situ* combustion method for the enhanced recovery of oil. The chemistry of aqueous aluminum ion at elevated temperatures is also of interest in connection with thermal methods of oil recovery, since the vast majority of minerals in the crustal rocks are aluminosilicates. Reaction of these minerals with hot aqueous fluids produced by steam injection or *in situ* combustion results in the formation of slightly soluble oxides that may adversely affect the hydrodynamic properties of the reservoir matrix. The aqueous chemistry of aluminum ion is also important for several other reasons, some of which are cited in the introduction to Chapter 1.

CHAPTER 1

Densities and Apparent Molar Volumes of Aqueous Aluminum Chloride.

Analysis of Apparent Molar Volumes and Heat Capacities of Aqueous

Aluminum Salts in terms of the Pitzer and Helgeson Theoretical Models

Introduction

The thermodynamic properties of aqueous aluminum ion are needed in applying chemical equilibrium models to mineral-water interactions relevant to geothermal processes, to *in situ* bitumen recovery processes, and to soil and clay mineral chemistry. Specific examples include the precipitation of protective oxide or hydroxide on otherwise reactive surfaces and the enhanced solubility of aluminum-containing minerals due to complexation and hydrolysis equilibria.

Some standard state thermodynamic properties (Gibbs free energy of formation, enthalpy of formation, and entropy) of $\text{Al}^{3+}(\text{aq})$ at 298.15 K and 1 bar are already available (1). To use these properties for equilibrium calculations that apply to high temperature or high pressure systems, we also need the standard state partial molar heat capacity and volume of $\text{Al}^{3+}(\text{aq})$, which are the principal subjects of this chapter. In addition, the heat capacity and volume (temperature and pressure derivatives of the Gibbs free energy) are useful in

connection with theoretical models for aqueous solutions (2-4) that are themselves applicable to the effective use of tabulated thermodynamic properties (298.15 K and 1 bar) for calculating properties at higher temperatures (5-8) and pressures (8-10).

Heat capacity data for aqueous solutions of aluminum chloride and nitrate have just recently become available (11), but have not yet been considered in relation to the Pitzer (2) and Helgeson (3-4) models, which is done in this chapter. Previously available volumetric data are limited to relative densities at 18°C of aqueous solutions of aluminum chloride and of aluminum nitrate (12) and of solutions of aluminum nitrate-nitric acid in the temperature range 0-60°C (12,13). Calculation (14-15) of the desired standard state partial molar volumes of the aluminum salts from these results (12,13) is complicated in the first case by hydrolysis and in the second by substantial mixed electrolyte effects. Possibly because of these complications or possibly because of errors in the original experimental results, the standard state partial molar volumes of $\text{Al}^{3+}(\text{aq})$ at 25°C derived from these earlier results differ by about $2 \text{ cm}^3 \text{ mol}^{-1}$. New measurements of the densities of solutions of aluminum chloride-hydrochloric acid therefore were made. Results of these measurements of densities and measurements of heat capacities by Hovey and Tremaine (11) have been used for the extrapolation from finite concentration to the infinitely dilute reference state and in connection with theoretical models for the concentration, temperature, and pressure dependence of thermodynamic properties of aqueous electrolytes. More specifically, the Pitzer (2)

ion-interaction model and the Helgeson, Kirkham, and Flowers⁽⁴⁾ extended Debye-Huckel model have been used for extrapolation to infinite dilution, and the Helgeson and Kirkham⁽³⁾ electrostatic model has been applied to the temperature dependence of the standard state thermodynamic properties.

Experimental

Densities of solutions at 10, 25, 40, and 55°C were measured relative to the density of pure water at the same temperature with a Sodev 03D vibrating tube densimeter (16) fitted with a platinum tube. A CT-L/PC-B temperature controller provided temperature stability of 0.001 K. The densimeter was calibrated with distilled water and standard solutions of 1 m NaCl prepared by mass from Fisher ACS Certified crystals dried overnight at 110°C. Densities of 0.1 m NaCl solutions prepared from this standard were measured periodically to monitor reliability of the instrument's performance. Calibrations at 25°C were based on the density of water from Kell (17) and densities of solutions of NaCl from Fortier, Leduc, and Desnoyers (18). Densities of water and solutions of NaCl at other temperatures were taken from Haar, Gallagher, and Kell (19), and Rogers and Pitzer (20), respectively.

A stock solution was prepared by dissolving approximately 90 g of Alfa Puratronic $\text{AlCl}_3 \cdot 6\text{H}_2\text{O}$ in 720 g of standard 0.015 M HCl. Aluminum was determined gravimetrically as the 8-hydroxyquinolate, with results from which it was calculated that the stock solution was 0.4962 ± 0.0006 molal in Al^{3+} .

Preliminary pH measurements on a 0.5 m solution of $\text{AlCl}_3 \cdot 6\text{H}_2\text{O}$ in distilled water indicated that the amount of HCl occluded in the solid was less than the estimated relative error of a gravimetric chloride determination. The HCl standard solution was therefore assumed to be the sole source of H^+ in the acidic solution of aluminum chloride, and the molality of chloride was calculated by difference.

A series of solutions of AlCl_3 in the composition range 0.03-0.5 m was obtained by diluting the stock solution by mass with standard 0.001 M HCl. Volumetric data for aqueous HCl (18) allowed calculation of solution compositions on a mass (molality, m) basis.

Water used as reference liquid and as solvent was singly distilled, de-ionized, filtered through activated carbon to remove organic contaminants, and boiled to remove dissolved gases.

Results and Calculations

For treatment of densities of the mixed electrolyte (AlCl_3 and HCl) we follow principles summarized by Millero (21) in defining a mean apparent molar volume as

$$[1-1] \quad V_\phi(\text{mean}) = (V - 1000v_w)/\sum m_i$$

in which V is the total volume (cm^3) of a solution containing 1 kg of water, v_w is the volume of 1 g of water, and the m_i represent molalities of solutes i . Eq. [1-1]

leads to

$$[1-2] \quad V_{\phi}(\text{mean}) = [1000(d_w - d) + d_w \sum m_i W_i] / [d_w \sum m_i]$$

in which d and d_w represent the densities of solution and pure water, respectively, and the W_i represent the molar masses of solutes i .

Compositions and densities of the solutions are given in the first three columns in Table 1-1, with mean apparent molar volumes calculated according to eq. [1-2] given in the fourth column.

Because the fraction of the total ionic strength due to the aluminum chloride greatly exceeds that due to the hydrochloric acid in our solutions, we can attempt to isolate the defined apparent molar volume for each solute by application of Young's rule (22), which may be written as

$$[1-3] \quad (m_j + m_k) V_{\phi}(\text{mean}) = m_j V_{\phi}(\text{AlCl}_3) + m_k V_{\phi}(\text{HCl})$$

where m_j and m_k refer to the molalities of aqueous AlCl_3 and HCl , respectively.

Use of eq. [1-3] with the experimental results (Table 1-1) and the volumetric properties of aqueous HCl from Akerlof and Teare (23) has led to the desired values of $V_{\phi}(\text{AlCl}_3)$ that are listed in the fifth column in Table 1-1. We can in

principle use these calculated values of $V_{\phi}(\text{AlCl}_3)$ in an extended Debye-Huckel equation of the form

$$[1-4] \quad V_{\phi} = V_{\phi}^0 + A_V m^{1/2} + B_V m + \dots \quad (\text{or ionic strength, } I, \text{ instead of } m)$$

Table 1-1. Compositions and densities of aqueous mixtures of aluminum chloride and hydrochloric acid

m_j	m_k	$(d - d_w)$ $\times 10^2$	$(m_j + m_k)/m_j$ $\times V_\phi(\text{mean})$	$V_\phi(\text{AlCl}_3)$
mol kg^{-1}	mol kg^{-1}	g cm^{-3}	$\text{cm}^3 \text{mol}^{-1}$	$\text{cm}^3 \text{mol}^{-1}$
<u>10°C</u>				
0.4962	0.0160	5.6811	18.91	18.35
0.3456	0.0113	4.0114	17.73	17.15
0.2015	0.0065	2.3764	16.16	15.59
0.1460	0.0053	1.7377	15.30	14.65
0.1073	0.0041	1.2855	14.74	14.06
0.0795	0.0032	0.9572	14.20	13.47
0.0481	0.0023	0.5858	13.26	12.41
0.0299	0.0017	0.3667	12.74	11.71
<u>25°C</u>				
0.4962	0.0160	5.6065	20.11	19.55
0.3456	0.0113	3.9593	18.94	18.35
0.3456	0.0113	3.9586	18.96	18.37
0.2015	0.0065	2.3463	17.36	16.77
0.1460	0.0053	1.7154	16.54	15.87
0.1073	0.0041	1.2694	15.95	15.24
0.0795	0.0032	0.9453	15.40	14.64
0.0481	0.0023	0.5782	14.55	13.66
0.0299	0.0017	0.3631	13.65	12.57
0.0299	0.0017	0.3627	13.78	12.70

Table 1-1 (continued)

m_j	m_k	$(d - d_w)$ $\times 10^2$	$(m_j + m_k)/\bar{m}_j$ $\times V_\phi(\text{mean})$	$V_\phi(\text{AlCl}_3)$
mol kg^{-1}	mol kg^{-1}	g cm^{-3}	$\text{cm}^3 \text{mol}^{-1}$	$\text{cm}^3 \text{mol}^{-1}$
<u>40°C</u>				
0.4962	0.0160	5.5745	20.30	19.74
0.3456	0.0113	3.9368	19.13	18.53
0.2015	0.0065	2.3360	17.39	16.78
0.1460	0.0053	1.7075	16.59	15.90
0.1073	0.0041	1.2648	15.88	15.15
0.0795	0.0032	0.9435	15.13	14.35
0.0481	0.0023	0.5806	13.53	12.62
0.0299	0.0017	0.3628	13.22	12.11
<u>55°C</u>				
0.4962	0.0160	5.6666	17.89	17.34
0.3456	0.0113	3.9915	16.94	16.35
0.2015	0.0065	2.3623	15.42	14.81
0.1460	0.0053	1.7249	14.72	14.03
0.1073	0.0041	1.2793	13.81	13.08
0.0795	0.0032	0.9514	13.42	12.63
0.0481	0.0023	0.5854	11.78	10.86

to obtain the desired standard state partial molar volume represented here by V_{ϕ}^0 . But there are ambiguities as to the appropriate use of the molality of AlCl_3 or the total ionic strength and also other difficulties. Similar problems arise in connection with application of the Helgeson, Kirkham, and Flowers model (4). It is therefore preferable to use the Pitzer model (2,24), which explicitly deals with ionic interactions in mixed electrolyte solutions.

As the first step toward applying the Pitzer model to obtaining the standard state partial molar volume of the aqueous aluminum salt, $V^0(\text{AlCl}_3)$, from the experimentally based mean apparent molar volumes in Table 1-1, we define the excess volume of a solution as

$$[1-5] \quad V^{\text{EX}} = V - \sum n_i V^0(i)$$

in which the n_i and $V^0(i)$ are the numbers of moles and the standard state partial molar volumes of components i , respectively. Combination of eq. [1-4] and [1-5] leads to

$$[1-6] \quad V_{\phi}(\text{mean}) = (\sum m_i V^0(i) + V^{\text{EX}}) / \sum m_i$$

We now go from the general eq. [1-6] to the corresponding specific equation for two electrolytes represented by j and k as in eq. [1-3].

Rearrangement of the resulting specific version of eq. [1-6] gives

$$[1-7] \quad [(m_j + m_k)V_{\phi}(\text{mean}) - m_k V^0(k)] / m_j = V^0(j) + (V^{\text{EX}} / m_j)$$

The excess volume, V^{EX} , may be represented directly as the pressure

derivative of the excess Gibbs free energy as developed by Pitzer and others (2,24,25). For a ternary common ion system resulting from mixing electrolytes MX_3 and NX of charge types 3:1 and 1:1, respectively, the interaction model representation, per kilogram of water, may be written

$$[1-8] \quad G^{EX}/RT = f^{GX}(I) + 2m_c m_j (B_{MX} + C_{MX} m_c) + 2m_c m_k (B_{NX} + C_{NX} m_c) + m_j m_k (\theta_{MN} + m_c \phi_{MNX})$$

where I is ionic strength, m_j and m_k are molalities of electrolytes MX_3 and NX in the mixture, and m_c is the molality of the common ion X . All other symbols are as previously defined (24). Because the pressure derivatives of C_{MX} and the mixing coefficients, θ_{MN} and ϕ_{MNX} , are too small to be important in our concentration range, we have assigned these parameters values of zero. Substituting the pressure derivative of eq. [1-8], modified as stated, into eq. [1-7] and rearranging gives

$$[1-9] \quad V_\phi (m_j + m_k)/m_j - (m_k/m_j) [V^0(HCl) + 2RTm_c(B_{HCl}^V + C_{HCl}^V m_c)] - \{A_V I \ln(1 + 1.2 I^{1/2})\} / (1.2 m_j) = V^0(AlCl_3) + 2RTm_c B_{AlCl}^V$$

The binary interaction coefficient, B^V , has an ionic strength dependence originally defined for the osmotic coefficient (2). For the excess Gibbs free energy the appropriate function is

$$[1-10] \quad B^{GX} = \beta^{(0)} + \beta^{(1)} [1 - (1 + 2 I^{1/2}) \exp(-2 I^{1/2})] / (2 I)$$

$V^0(\text{AlCl}_3)$, $\beta^{(1)V}$, and $\beta^{(0)V}$ were evaluated at each temperature by multiple linear regression analysis of the density data using eq. [1-9] and [1-10] and values of B_{HCl}^V and C_{HCl}^V calculated from data (23) for aqueous HCl. The Debye-Huckel slope, A_V , is from Bradley and Pitzer (26). Values of the parameters for HCl are reported in Table 1-2. The desired resulting values of $V^0(\text{AlCl}_3)$ at the four temperatures of the measurements are listed in Table 1-3.

The values of $V^0(\text{AlCl}_3)$ were weighted statistically and then fit with an empirical function of temperature. Smoothed values calculated from this function were used to obtain final estimates of the parameters $\beta^{(1)V}$ and $\beta^{(0)V}$. The former was fit with an empirical function of temperature, and the latter was represented by a Lagrange polynomial. The result is that the temperature dependence of the parameters for volumetric properties of AlCl_3 over the range 10-55°C may be represented by the following equations:

$$[1-11] \quad V^0(\text{AlCl}_3) = a_1 + a_2T + a_3T^2$$

$$[1-12] \quad \beta^{(1)V} = a_4 + a_5T + a_6/(T-362)$$

$$[1-13] \quad \beta^{(0)V} = a_7T^3 + a_8T^2 + a_9T + a_{10}$$

Values of the coefficients $a_1 \dots a_{10}$ are listed in Table 1-4. The temperature dependence of the interaction parameters is shown in Fig. 1-1.

Table 1-2. Smoothed Pitzer interaction model parameters for apparent molar volumes of HCl estimated from the fit to data from Akerlöf and Teare (23)

Temperature	$V^0(\text{HCl})$	σ^*	$\beta^{(1)}V$	$\beta^{(0)}V$	CV
$^{\circ}\text{C}$	$\text{cm}^3 \text{ mol}^{-1}$		$\times 10^5$	$\times 10^5$	$\times 10^6$
10	17.15	0.04	3.60	-2.39	-1.63
25	17.95	0.06	4.96	-3.57	-2.11
40	18.35	0.07	5.99	-4.43	-2.49
55	18.34	0.10	6.85	-5.12	-2.83

* Standard error of the estimate at the 95% confidence level

Table 1-3. Standard partial molar volume of aqueous AlCl_3 obtained by extrapolation using the Pitzer interaction model

Temperature	$V^0(\text{AlCl}_3)$	σ^*
$^{\circ}\text{C}$	$\text{cm}^3 \text{ mol}^{-1}$	
10	8.25	0.22
25	8.81	0.25
40	8.05	0.28
55	6.05	1.05

* Standard error of the estimate at the 95% confidence level

Table 1-4. Coefficients for apparent molar volume of AlCl_3 (eq. [1-11]-[1-13])

Coefficient	Estimate
a_1	-2.3026×10^2
a_2	1.6126
a_3	-2.7193×10^{-3}
a_4	-9.8574×10^{-4}
a_5	4.6327×10^{-6}
a_6	2.4396×10^{-2}
a_7	-4.63825×10^{-10}
a_8	4.30964×10^{-7}
a_9	-1.33542×10^{-4}
a_{10}	1.38003×10^{-2}

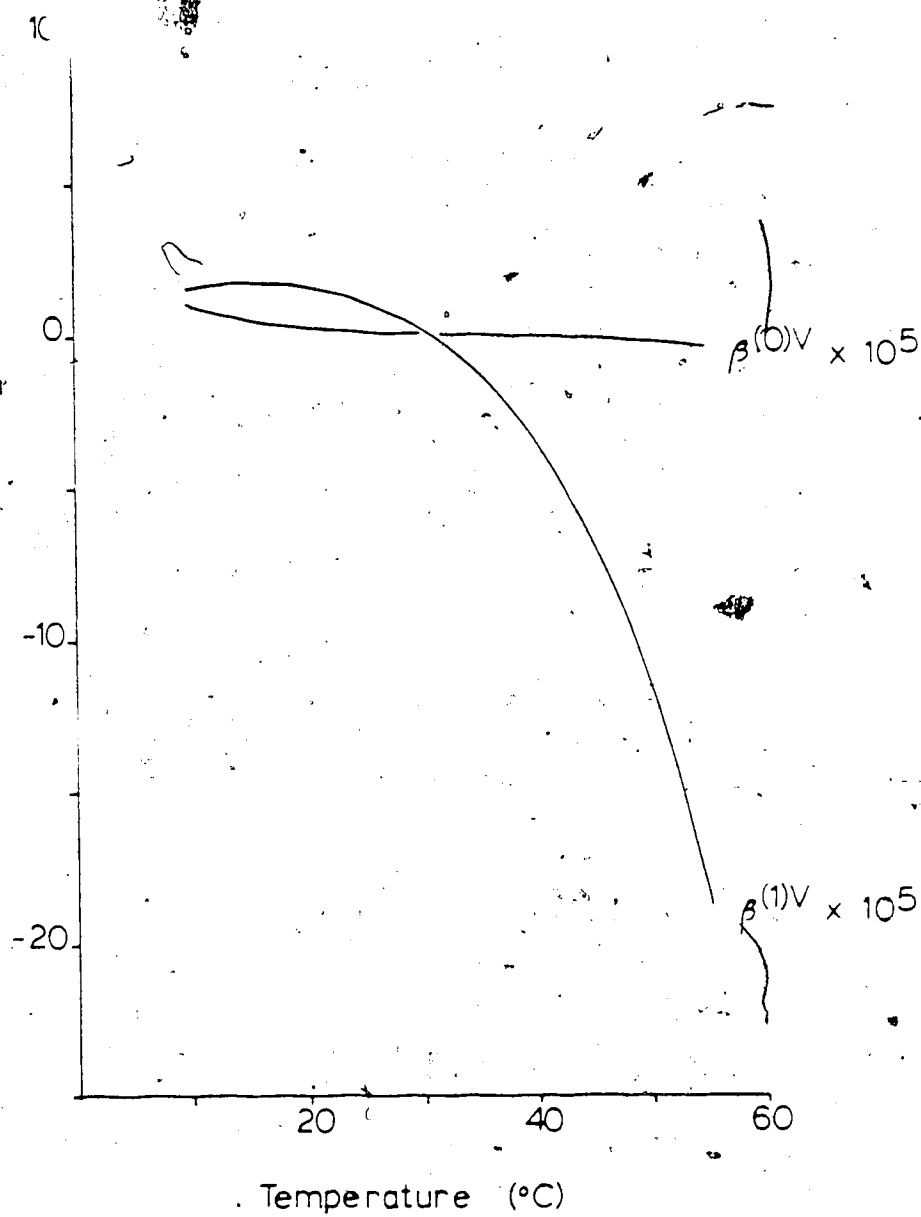


Figure 1-1. Temperature dependence of binary interaction parameters for the apparent molar volume of aluminum chloride from 10-55°C.

A set of equations based on the Pitzer virial model can be developed similarly for analyzing and representing other apparent molar properties. In this work we have carried out such development for the apparent molar heat capacity and have applied the resulting equations to the data of Hovey and Tremaine (11) for $\text{AlCl}_3\text{-HCl}$ mixtures at temperatures of 10, 25, 40, and 55°C. As in the case of volumes, the mixing parameters may be neglected. The excess heat capacity is

$$[1-14] \quad C_p^{\text{EX}} = -T(\partial^2 G^{\text{EX}}/\partial T^2)_{p,X}$$

Combination of eq. [1-14] and [1-8] with the general form of eq. [1-7] leads to a regression model for evaluating $C_p^0(\text{AlCl}_3)$ and the second temperature derivatives of the interaction parameters:

$$[1-15] \quad C_{p,\phi} (m_j + m_k)/m_j - (m_k/m_j) [C_p^0(\text{HCl}) - 2RT^2 m_c (B_{\text{HCl}}^J + C_{\text{HCl}}^J m_c)] \\ - [A_J | \ln(1 + 1.2 | 1/2) | / (1.2 m_j)] = C_p^0(\text{AlCl}_3) - 2RT^2 m_c [B_{\text{AlCl}_3}^J + \\ (\sqrt{3}/3) C_{\text{AlCl}_3}^J m_c]$$

Values of $C_p^0(\text{HCl})$ and B_{HCl}^J were calculated from the equations of Tremaine, Sway, and Barbero (8) and are listed in Table 1-5. Data for evaluating C_{HCl}^J are not yet available, and this parameter was tentatively assigned a value of zero. Values of $C_{p,\phi}(\text{mean})$ were taken as reported (11).

The Debye-Huckel slope, A_J , is from Bradley and Pitzer (26).

In addition to the intercept, $C_p^0(\text{AlCl}_3)$, which is the desired quantity, only the $\beta^{(1)J}$ term was needed to fit the heat capacity data. The temperature dependence of this parameter and also that of $C_p^0(\text{AlCl}_3)$ were fit with the following empirical functions:

$$[1-16] \quad C_p^0(\text{AlCl}_3) = b_1 + b_2T + b_3/(T-190)$$

$$[1-17] \quad \beta^{(1)J} = b_4 + b_5T + b_6/(T-190)$$

Values of the coefficients $b_1 \dots b_6$ are listed in Table 1-6. Fig. 1-2 shows the temperature dependence of $\beta^{(1)J}$. Values of $C_p^0(\text{AlCl}_3)$ at the four temperatures of the measurements are listed in Table 1-7.

We turn now to the representation of the standard state properties of aluminum ion, $V^0(\text{Al}^{+3})$ and $C_p^0(\text{Al}^{+3})$, as semi-theoretical functions of temperature that can be combined with other data, as stated in the Introduction, for use in equilibrium calculations at elevated pressures and temperatures. For this purpose we have chosen the equations of Helgeson and Kirkham (3), which express the standard state properties of ions as the sum of terms describing low temperature electrostrictive collapse of the solvent structure and the change in hydration at high temperature due to rapid decrease in the dielectric constant of water. At constant pressure the appropriate relations are

Table 1-5. Smoothed Pitzer interaction model parameters for apparent molar heat capacities of HCl calculated from the equations given by Trémaine, Sway, and Barbero (8)

Temperature	$C_p^0(\text{HCl})$	$\beta^{(0)}J \times 10^5$
$^{\circ}\text{C}$	$\text{J mol}^{-1} \text{K}^{-1}$	
10	-148.3	-8.48
25	-126.6	-1.35
40	-115.5	0.03
55	-111.7	0.19

Table 1-6. Coefficients for apparent molar heat capacity of AlCl_3 (eq. [1-16] and [1-17])

Coefficient	Estimate
b_1	2.9801×10^3
b_2	-7.3388
b_3	-1.3915×10^5
b_4	4.3122×10^{-3}
b_5	-8.6428×10^{-6}
b_6	-1.7424×10^{-1}

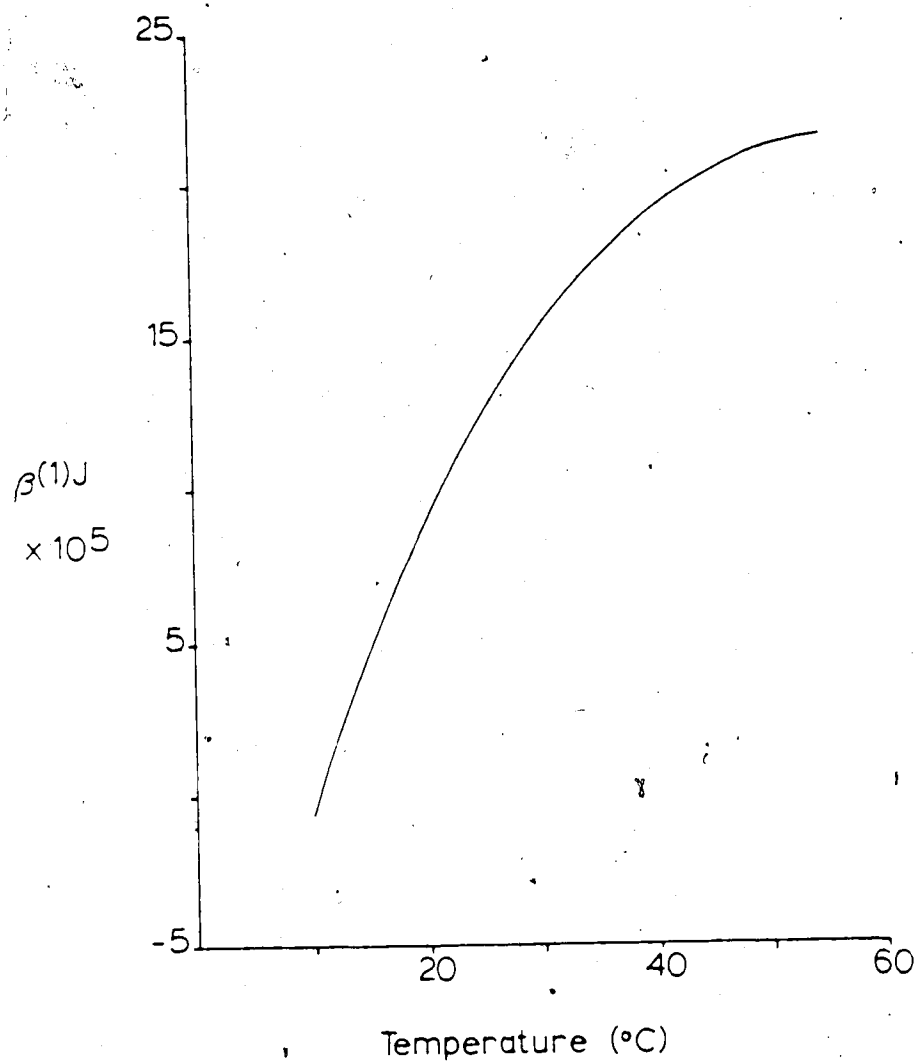


Figure 1-2. Temperature dependence of binary interaction parameter for the apparent molar heat capacity of aluminum chloride from 10-55°C.

Table 1-7. Standard partial molar heat capacities of $\text{AlCl}_3(\text{aq})$ obtained by extrapolation using the Pitzer interaction model

Temperature	$C_p^\circ(\text{AlCl}_3)^\circ$	σ^*
$^\circ\text{C}$	$\text{J mol}^{-1} \text{K}^{-1}$	
10	-591.8	16.8
25	-493.8	6.3
40	-448.1	9.4
55	-433.3	18.8

* Standard error of the estimate at the 95% confidence level

Table 1-8. Coefficients for the Helgeson-Kirkham model for the standard state partial molar properties of $\text{Al}^{3+}(\text{aq})$ (eq. [1-18,19])

Coefficient	Estimate
c_1	-43.984
c_2	1.1606
d_1	135.54
d_2	-28.988
$\theta_{\text{Al}^{3+}}$	239.9 K

$$[1-18] \quad V^0(\text{Al}^{3+}) = c_1 + c_2 T / (T - \theta_{\text{Al}^{3+}}) - \omega_{\text{Al}^{3+}} - Q$$

$$[1-19] \quad C_p^0(\text{Al}^{3+}) = d_1 + d_2 T / (T - \theta_{\text{Al}^{3+}}) - \omega_{\text{Al}^{3+}} + T \chi$$

in which c_1 , c_2 , d_1 , and d_2 are adjustable parameters and $\theta_{\text{Al}^{3+}}$ is an adjustable "structural" temperature that allows a simple empirical description of the rapid decrease in the standard state properties, observed for many ions, with decreasing temperature in the low temperature region. The terms in $\omega_{\text{Al}^{3+}}$ are based on the Born hydration model and may be calculated from the following relations defined by Helgeson and Kirkham (3):

$$[1-20] \quad \omega_i = \eta z_i^2 / (r_{\text{xtl}} + 0.94 z_i) - 5.387 \times 10^4 z_i$$

$$[1-21] \quad Q = (1/D)(\partial \ln D / \partial p)_T$$

$$[1-22] \quad \chi = (1/D) [(\partial^2 \ln D / \partial T^2)_p - (\partial \ln D / \partial T)_p^2]$$

in which $\eta = 1.66027 \times 10^5 \text{ Å cal mol}^{-1}$, r_{xtl} is the crystallographic radius of the ion, and D is the dielectric constant of pure water. Eq. [1-18] and [1-19] in principle apply to ionic properties calculated on either the absolute or the conventional basis (assigning a value of zero to the corresponding property of hydrogen ion at each temperature). Because of the additional uncertainties involved in defining absolute thermodynamic properties of ions, we prefer to use conventional values and have chosen the corresponding form of ω_i , eq. [1-20], in which the coefficient of the last term is the absolute electrostatic Born

parameter for the hydrogen ion.

Combining the values of the standard state partial molar properties of AlCl_3 listed in Tables 1-3 and 1-7 with those for chloride ion based on the values for HCl listed in Tables 1-2 and 1-5, conventional values of $V^0(\text{Al}^{3+})$ and $C_p^0(\text{Al}^{3+})$ have been calculated. Table 1-8 reports the results of the simultaneous optimization of eq. [1-18] and [1-19] with respect to the common parameter, $\theta_{\text{Al}^{3+}}$, using the Pauling radius of Al^{3+} and values of Q and χ calculated from the equations of Bradley and Pitzer (26). The temperature dependences of the standard state properties of aluminum ion are shown in Fig. 1-3(a) and 1-3(b).

Discussion

The quantity on the right side of eq. [1-9] or [1-15] is equivalent to the difference between the apparent molar property of AlCl_3 as defined by Young's rule and that part of the Debye-Huckel term due to the aluminum salt. Values of this quantity calculated from the density and heat capacity data in combination with the information in Tables 1-2 and 1-5 and from the smoothed curves of the global fits (eq. [1-11] - [1-13] for volumes and eq. [1-17] and [1-19] for heat capacities) are plotted against molality of aluminum in Figs. 1-4 and 1-5. The accuracy of the Pitzer interaction model correlation of the data as described in the preceding section is within the limit of the overall experimental uncertainties. The quality of fit of the Helgeson and Kirkham model to the

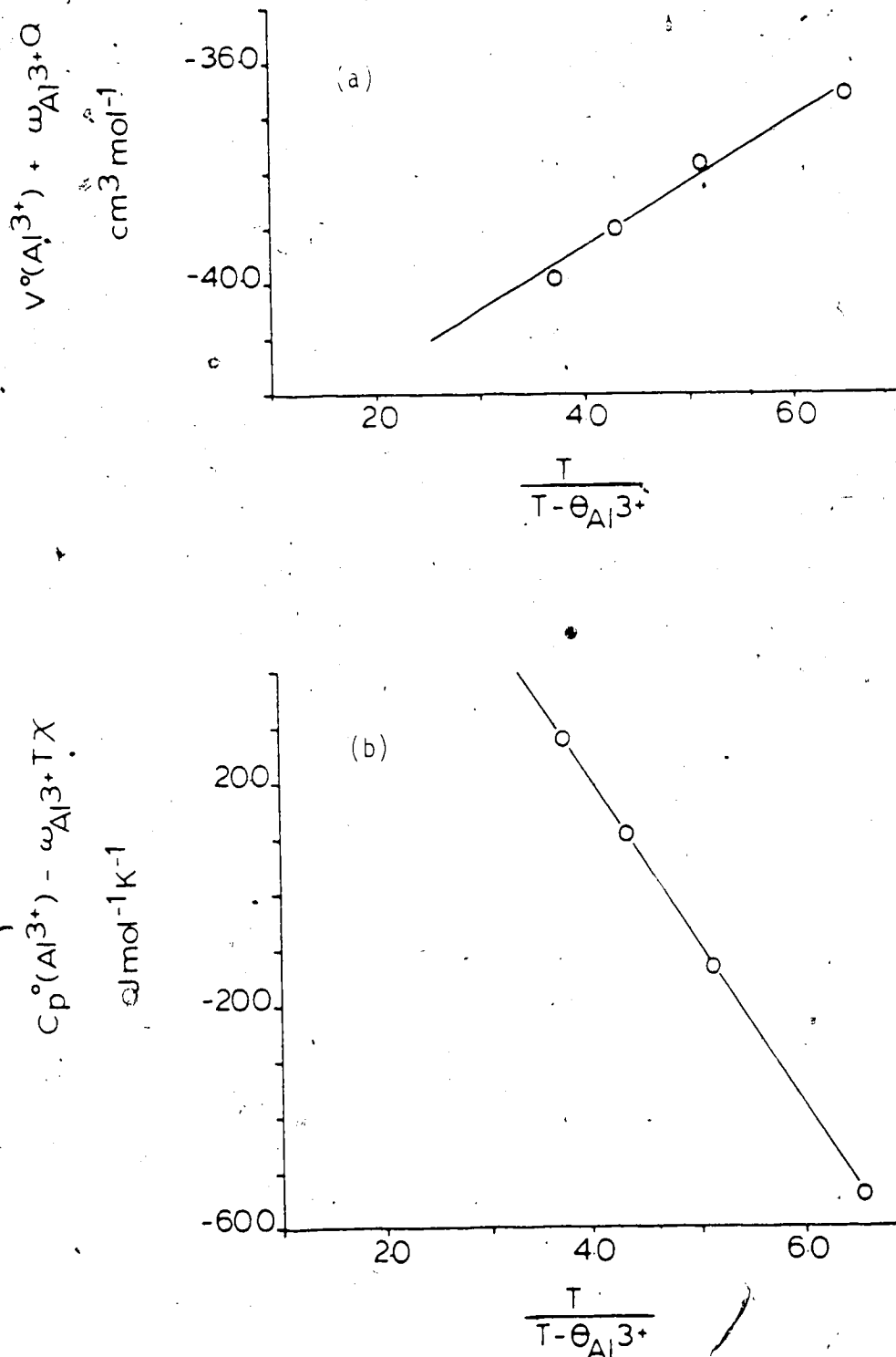


Figure 1-3: Temperature dependence of the standard partial molar (a) volume and (b) heat capacity of $\text{Al}^{3+}(\text{aq})$. Helgeson-Kirkham model representation (solid lines) of the extrapolated values (circles), corrected for the Born hydration contribution.

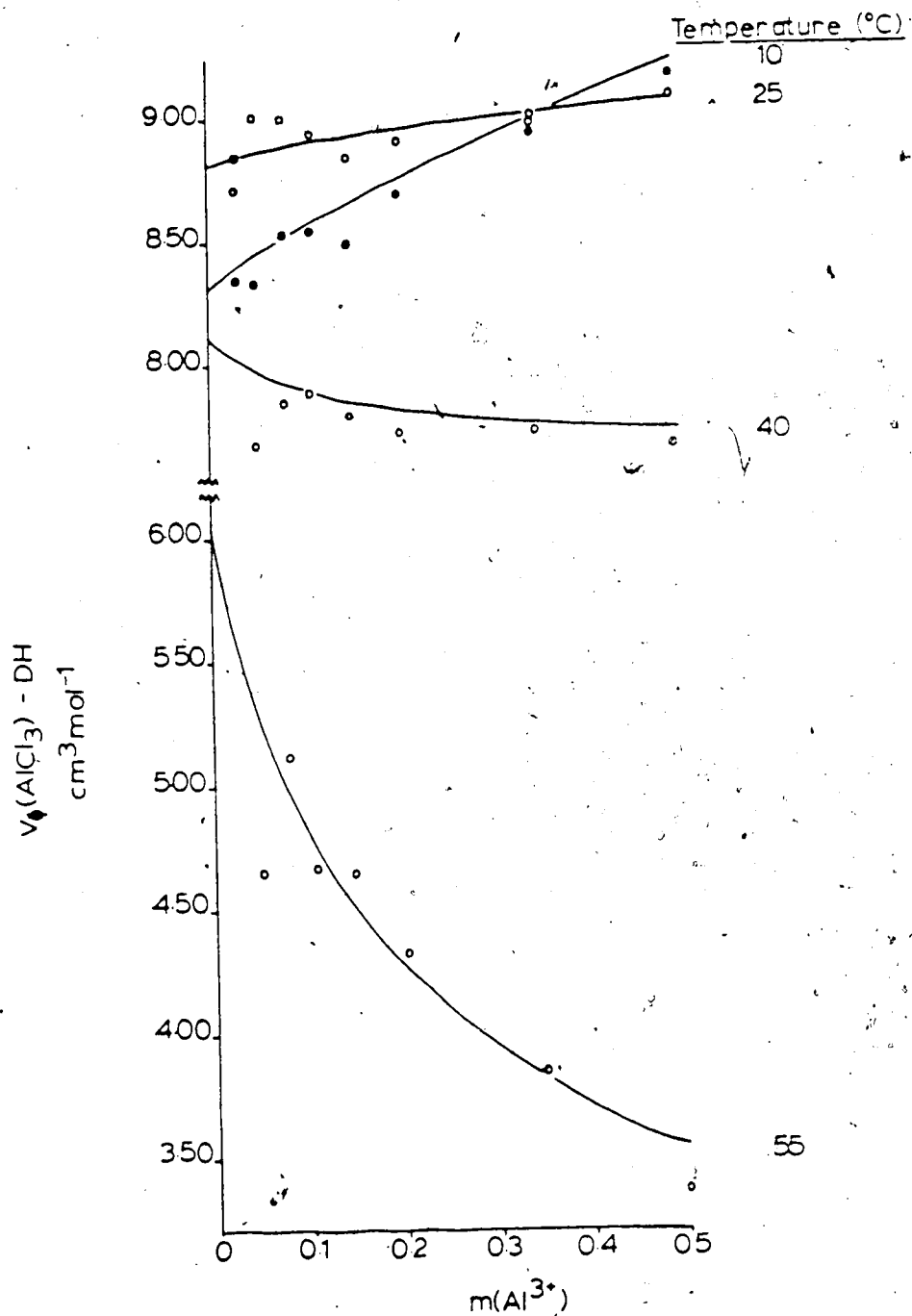


Figure 1-4. Apparent molar volume of aluminum chloride from 10-55°C, corrected for the Debye-Huckel electrostatic contribution. Solid curves are calculated from the fit of the Pitzer virial model.

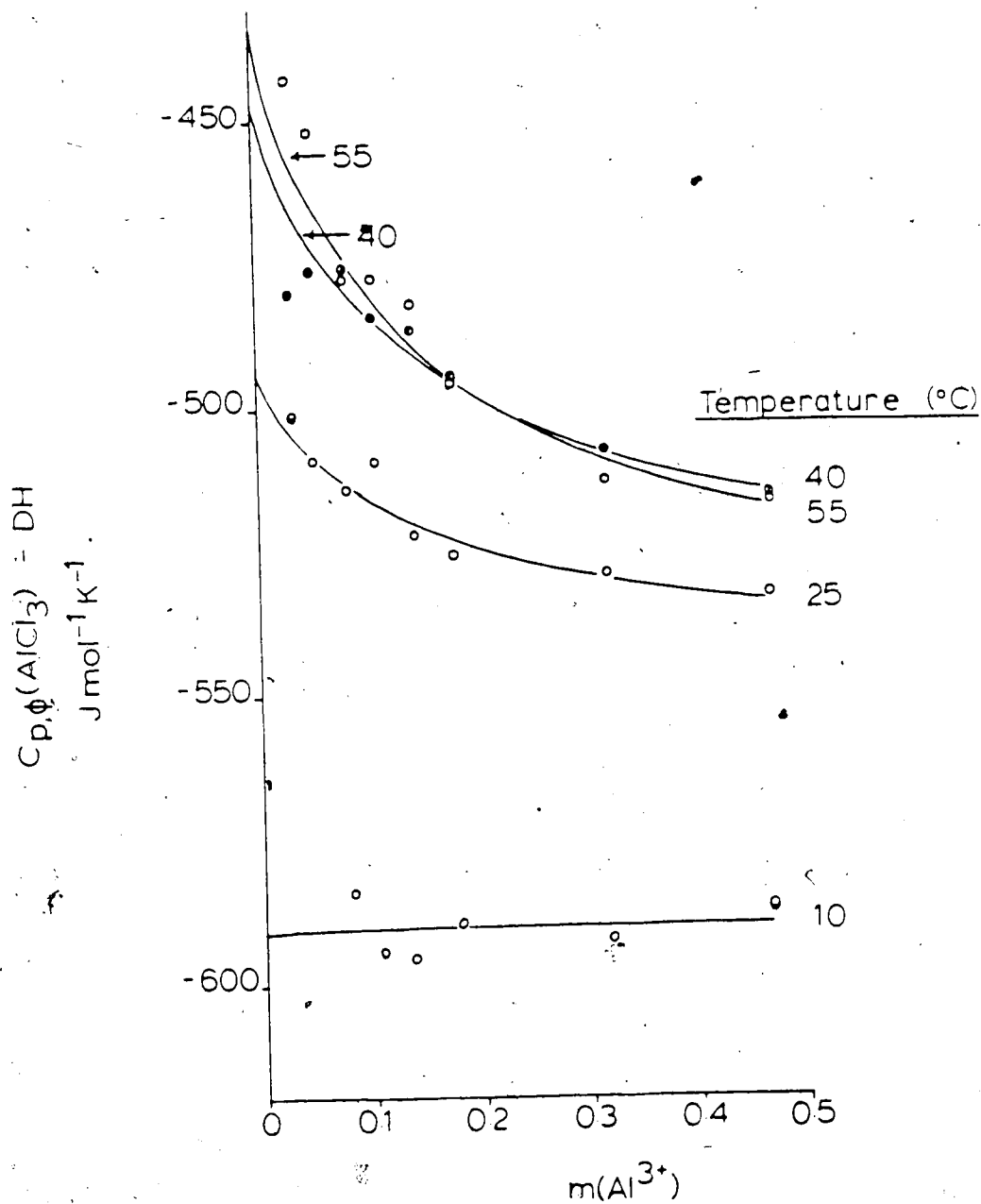


Figure 1-5. Apparent molar heat capacity of aluminum chloride from 10-55°C, corrected for the Debye-Huckel electrostatic contribution. Solid curves are calculated from the fit of the Pitzer virial model. Data (circles) are from Hovey and Tremaine (11).

standard state partial molar properties of aluminum ion is acceptable in the case of both volume (Fig. 1-3a) and heat capacity (Fig. 1-3b). Because no minimum relative sum of squares with respect to $\theta_{\text{Al}^{3+}}$ occurs in the objective function for the volume, the optimization is essentially governed by the heat capacity. The resulting value of $\theta_{\text{Al}^{3+}}$ (Table 1-8) leads to values of $V^0(\text{Al}^{3+})$ and $C_p^0(\text{Al}^{3+})$ within 0.6% ($0.25 \text{ cm}^3 \text{ mol}^{-1}$) and 0.9% ($0.9 \text{ J mol}^{-1} \text{ K}^{-1}$) of the respective calculated isothermal values. These differences are small enough that eq. [18] and [19] may reasonably be used in estimating the pressure and temperature dependence of equilibria involving $\text{Al}^{3+}(\text{aq})$ to perhaps 1 kbar and 200°C . Eq. [1-16] and [1-19] represent $C_p^0(\text{AlCl}_3)$ equally well; however, the empirical relation for $V^0(\text{AlCl}_3)$ (eq. [1-11]) is superior to the Helgeson-Kirkham model for the purpose of data representation.

Since only solute-solvent interactions contribute to the partial molar properties at infinite dilution, it is interesting to compare the values obtained in the preceding section for $\text{Al}^{3+}(\text{aq})$ calculated from the data for aluminum chloride with those that may be obtained from another aluminum salt. Using the equations developed in this paper, data for nitric acid from Enea *et al.* (27), and data for aluminum nitrate-nitric acid mixtures at 25°C from Hovey and Tremaine (11), Table 1-9 has been compiled. Both $C_p^0(\text{Al}^{3+})$ and $V^0(\text{Al}^{3+})$ obtained from the chloride are slightly more negative than the corresponding properties obtained from the nitrate, but both sets of values are coincident

within the limit of error at the 95% confidence level. The values of $V^0(\text{Al}^{3+})$ obtained by this analysis are in better agreement than are those that may be calculated similarly from results listed in Millero's compilation (15).

The values of the pressure derivatives of the interaction parameters for HCl (Table 1-2), HNO_3 (Table 1-9) and AlCl_3 (Figs. 1-1,2) all are small and similar in magnitude to values that have been reported for other 1:1 and 3:1 electrolytes (28,29). The small and nearly constant value of $\beta^{(0)V}$ for AlCl_3 indicates that the volumetric properties of the solutions do not change rapidly with temperature and that the predominant contribution to the excess volume is the long range Debye-Huckel term. The decrease in the value of $\beta^{(1)V}$ above 40°C is a consequence of the shift in the temperature at which V^0 is a maximum to lower temperature with decreasing ionic strength, combined with the essentially constant value of the more important parameter $\beta^{(0)V}$ over the temperature range 10 - 55°C . For electrolytes having a common anion, this shift is correlated with increase in surface charge density of the cation (29a,b). Thus for aqueous chlorides of sodium, calcium, and the trivalent rare earths, the temperature at which V^0 is maximum is 60 , 44 , and 27 - 31°C , respectively. AlCl_3 , with still higher cationic surface charge density, fits naturally into this sequence, with V^0 maximum at 25°C . The value of $\beta^{(1)V}$ for the rare earth chlorides at 25°C is approximately -2×10^{-4} , while $\beta^{(1)V}$ for AlCl_3 reaches this value only above 55°C .

Table 1-9. Pitzer interaction model parameters for apparent molar volumes and heat capacities of HNO_3 and $\text{Al}(\text{NO}_3)_3$ at 25°C : standard state partial molar properties of $\text{Al}^{3+}(\text{aq})$

Electrolyte	Coefficient(a)	Estimate(a)	$\sigma(\text{a,b})$	Source of data
HNO_3	$V^0(\text{HNO}_3)$	29.20	0.35	ref. 27
	$\beta(1)V$	6.50×10^{-5}		
	$\beta(0)V$	0		
	$C_p^0(\text{HNO}_3)$	-72.4	0.5	ref. 27
	$\beta(1)J$	0		
	$\beta(0)J$	-3.68×10^{-5}		
	$V^0(\text{Al}^{3+})$	-44.13	0.98	
	$C_p^0(\text{Al}^{3+})$	-114.2	6.3	ref. 11
$\text{Al}(\text{NO}_3)_3$	$V^0(\text{Al}(\text{NO}_3)_3)$	43.47	0.77	ref. 11
	$\beta(1)V$	-1.48×10^{-4}		
	$\beta(0)V$	0		
	$C_p^0(\text{Al}(\text{NO}_3)_3)$	-327.2	4.4	ref. 11
	$\beta(1)J$	-1.91×10^{-4}		
	$\beta(0)J$	2.11×10^{-5}		
	$V^0(\text{Al}^{3+})$	-44.13	0.98	
	$C_p^0(\text{Al}^{3+})$	-110.0	4.5	
AlCl_3	$V^0(\text{Al}^{3+})$	-45.04	0.27	this work
	$C_p^0(\text{Al}^{3+})$	-114.2	6.3	ref. 11

(a) Units are $\text{cm}^3 \text{mol}^{-1}$ and $\text{J mol}^{-1} \text{K}^{-1}$

(b) Standard error of the estimate at the 95% confidence level

CHAPTER 2

Construction and Testing of an Aneroid Calorimeter for Investigating the Rates of Slow Reactions, with Application to the Low Temperature Oxidation of Athabasca Bitumen

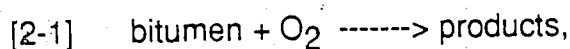
Introduction

In the *in situ* combustion method for the enhanced recovery of bitumen and heavy oils, air or oxygen is injected into the formation and part of the organic material is burned, producing heat and a variety of chemical products. Displacement of the remaining oil results from a number of physical and chemical processes, including reduction in viscosity due to increased temperature and dissolution of CO₂, thermal expansion, distillation and thermal cracking or pyrolysis, and increased pressure gradient due to the injected gas (30-36). Many investigators in this field of petroleum chemistry now recognize at least three major processes contributing to the global oxidation reaction described above: fuel (coke) formation due to distillation and pyrolysis, "low temperature oxidation" at temperatures below about 350°C, and "high temperature oxidation" at temperatures up to 500°C. Investigation of the rates and of the associated fuel and energy relationships in these processes provides some of the information needed to operate economically attractive *in situ* thermal projects.

At very low or at very high temperatures the rate of oxidation is either too slow or too fast to be of much interest in relation to *in situ* combustion processes. However, the rate of oxidation at the intermediate temperatures characteristic of the developing zone of combustion is of considerable practical importance. Earlier efforts to investigate the rate of oxidation in this intermediate temperature range, called "low temperature oxidation" or simply LTO, have focussed on measuring the rate of oxygen consumption and collecting and analyzing the produced gases (31,32,37-43).

More recently, differential scanning calorimetry (DSC) coupled with differential thermal analysis (DTA) or with thermogravimetric analysis (TGA) has been applied to the study of the rate of the global oxidation reaction, over temperatures ranging from ambient to several hundred degrees Celsius (33-36,44-53). In the thermal techniques mentioned here, energy changes in the substance of interest are measured continuously as the substance is heated at some predetermined rate, usually on the order of $10^{\circ}\text{C}/\text{min}$, over the desired range of temperature. The differential techniques measure this change relative to that of some standard substance. In general three peaks are observed, one near 200°C attributed to the onset of LTO, one near $300\text{-}350^{\circ}\text{C}$ attributed to high temperature oxidation, and one near 500°C attributed to thermal cracking. Extraction of kinetic parameters from the resulting thermograms is not straightforward and requires some preliminary assumptions about the sequence and relative importance of the various processes involved and about suitable kinetic models describing these processes.

Nearly all of the work cited here proceeds on the assumption that the global oxidation reaction,



can be represented as a sum of the major processes of thermal cracking, low temperature oxidation, and high temperature combustion, each conceived as an elementary reaction for which the rate constant is described by the Arrhenius equation,

$$[2-2] \quad k = A \exp(-E_a/RT),$$

in which A is the pre-exponential or frequency factor, E_a is the activation energy, R is the gas constant, and T is temperature in kelvins.

Fassihi *et al.* (41) and Yoshiki and Phillips (50) have summarized the results of a number of studies, both chemical and thermal, and have reported activation energies and corresponding reaction orders with respect to both fuel concentration and oxygen partial pressure for the low temperature oxidation of various crude oils and bitumens. Activation energies range from about 45-90 kJ/mol, reaction order with respect to fuel concentration is variously reported as either zero or unity, sometimes two, and reaction order with respect to oxygen concentration or partial pressure ranges from 0.3 to unity. Some investigators have suggested that specific surface area of fuel, rather than bulk fuel concentration, is the more appropriate variable in the representation of the reaction rate (31,32,36,45-48,51) on the basis that products adsorbed on the surface may hinder further oxidation or that the reaction occurs at the fuel/gas

interface.

Some of the discrepancies in reported values of the kinetic parameters may arise in part from the differences in properties and compositions of the individual bitumens and crude oils, including thermal and oxidative history. Some of these discrepancies may also result from the different thermal and oxidative histories imposed by different experimental conditions. In the DSC and other non-isothermal methods, for example, the LTO phase of the global oxidation occurs simultaneously with distillation and is completed in about 30 min, while in the isothermal flow method some distillation may occur prior to oxidation and reaction times vary from several hours to several days. In addition, there is some concern that representative results are difficult to obtain because of the very small sample sizes (1-3 mg of active material for DSC, a few tens of mg of active material for TGA) (54). A more serious difficulty with non-isothermal methods is that the temperatures of fuel (coke) formation and fuel combustion are not coincident. As a result, these methods cannot distinguish fuel availability from fuel consumption. Because both the amount and the quality of fuel available change with temperature, Bae (44) has argued that use of an Arrhenius equation in this context is not justified, particularly for low temperature oxidation.

To address some of these difficulties and unanswered questions we have designed and built an aneroid calorimeter with which the rate of heat production can be measured under nearly isothermal conditions. This chapter gives a detailed description of the calorimetric apparatus and method of

- measuring rates of oxidation. In testing this method, the Arrhenius equation has been applied to the analysis of results of systematic tests of the apparatus at two temperatures, yielding kinetic parameters for low temperature oxidation that may be compared with some of the published values cited in this introduction.

Experimental

Materials

The calorimeter (Fig. 2-1) consists of a thin-walled aluminum combustion tube 5 mm in I.D. and 40 cm in length mounted lengthwise through the center of a cylindrical aluminum block 14 cm in length and 4 cm in diameter. This block has two holes, parallel to the combustion tube and diametrically opposed, which contain a heater for calibration with electrical energy and a calibrated platinum resistance thermometer for measuring temperature. Two concentric cylindrical shells of pyrex glass, 8.5 and 6.0 cm in I.D. and 20 cm in length, both wrapped with aluminum foil, reduce convective and radiative heat losses from the calorimeter to the surrounding constant temperature furnace. A cylindrical aluminum block of mass roughly five times that of the calorimeter is mounted at each end of the combustion tube to absorb thermal fluctuations in the furnace and to improve thermal equilibrium of flowing gas with the surroundings.

In order to avoid uncertainties in our measurements due to possible catalytic effects of matrix mineralogy, as reported by others (45,48), the samples used in this investigation were "reconstructed tar sand" prepared by loading

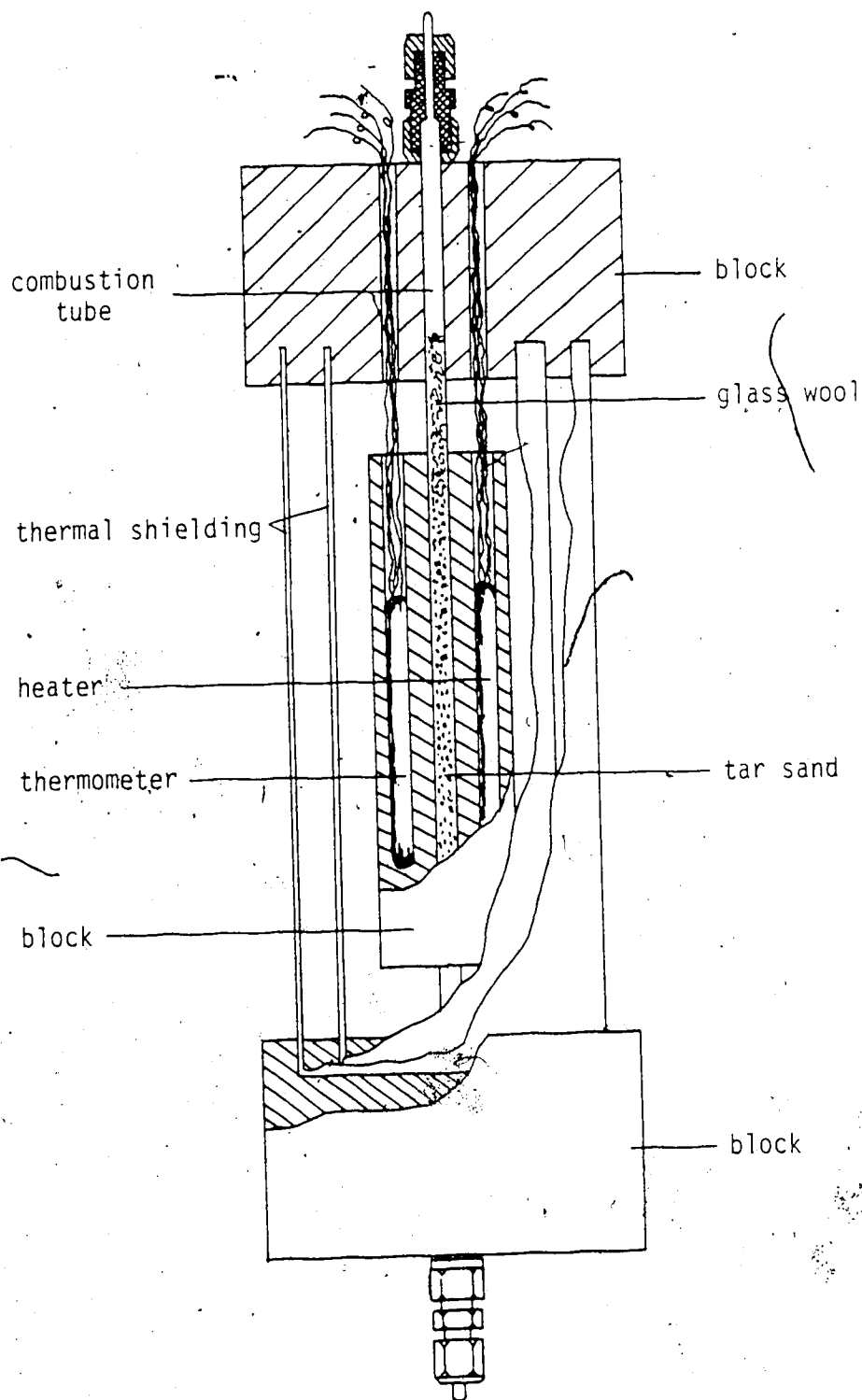


Figure 2-1. Partial section of aneroid calorimeter.

Athabasca bitumen onto 60/80 mesh (250-300 μm) Chromosorb-W acid-washed chromatographic support material, a substance of nearly pure silica. Preparation of approximately 100 g of tar sand was accomplished by adding about 87 g of the support material to a solution of about 13 g of bitumen in toluene, followed by flash evaporation of the solvent. The composition of the sample was determined gravimetrically by ashing in a muffle furnace at 750°C for 3 hr. Simultaneous ashing of bitumen and Chromosorb allowed calculation of the sample composition corrected for mass loss due to Chromosorb and mass residue due to ash. Subsamples of the tar sand were used in each calorimetric experiment.

Since the total heat released in a calorimetric experiment depends on the mass of active material present and since the rate at which this heat is released is expected to vary approximately exponentially with temperature, the optimum sample composition is that which has the maximum mass of bitumen per mass of sand and which, at the same time, does not have so much bitumen that displacement by gas flow occurs. This optimum composition was found to be about 13% bitumen by mass. A convenient sample size is about 1 g, containing approximately 100 mg of active material. The sample is placed in the combustion tube and held in position by two plugs of glass wool.

Operation

The combustion tube is connected with swaged brass fittings to a stainless steel gas train. This gas train (Fig. 2-2) allows either nitrogen or oxygen to flow through the combustion tube and through adsorption tubes that collect water and acidic products evolved during oxidation of the bitumen. The volume flow rate is measured prior to discharging the exhaust gases to a fume hood. Pressure upstream and downstream from the calorimeter is measured with a Heise pressure gauge (model 711B) with digital readout accurate to ± 0.1 kPa over a range of 0-500 kPa.

The calorimeter, charged with the reconstructed tar sand, is placed horizontally in an oven (Hotpack, model 213023) and flushed with nitrogen for about 18 hr to remove all traces of air from the sample and gas train. The oven is then brought to the temperature of interest. When the temperature of the calorimeter stabilizes several hours later, oxygen is admitted to the system and the resulting temperature rise due to heat produced by oxidation of the bitumen is recorded continuously on a strip chart until the temperature of the calorimeter returns to the constant temperature of the oven. Thermal stability of the oven is $\pm 0.1^\circ\text{C}$ over a range of 40-350°C.

Analysis of Data

Calibration

In order to transform the record of temperature rise versus time into the desired relationship between rate of production of heat and time, we have

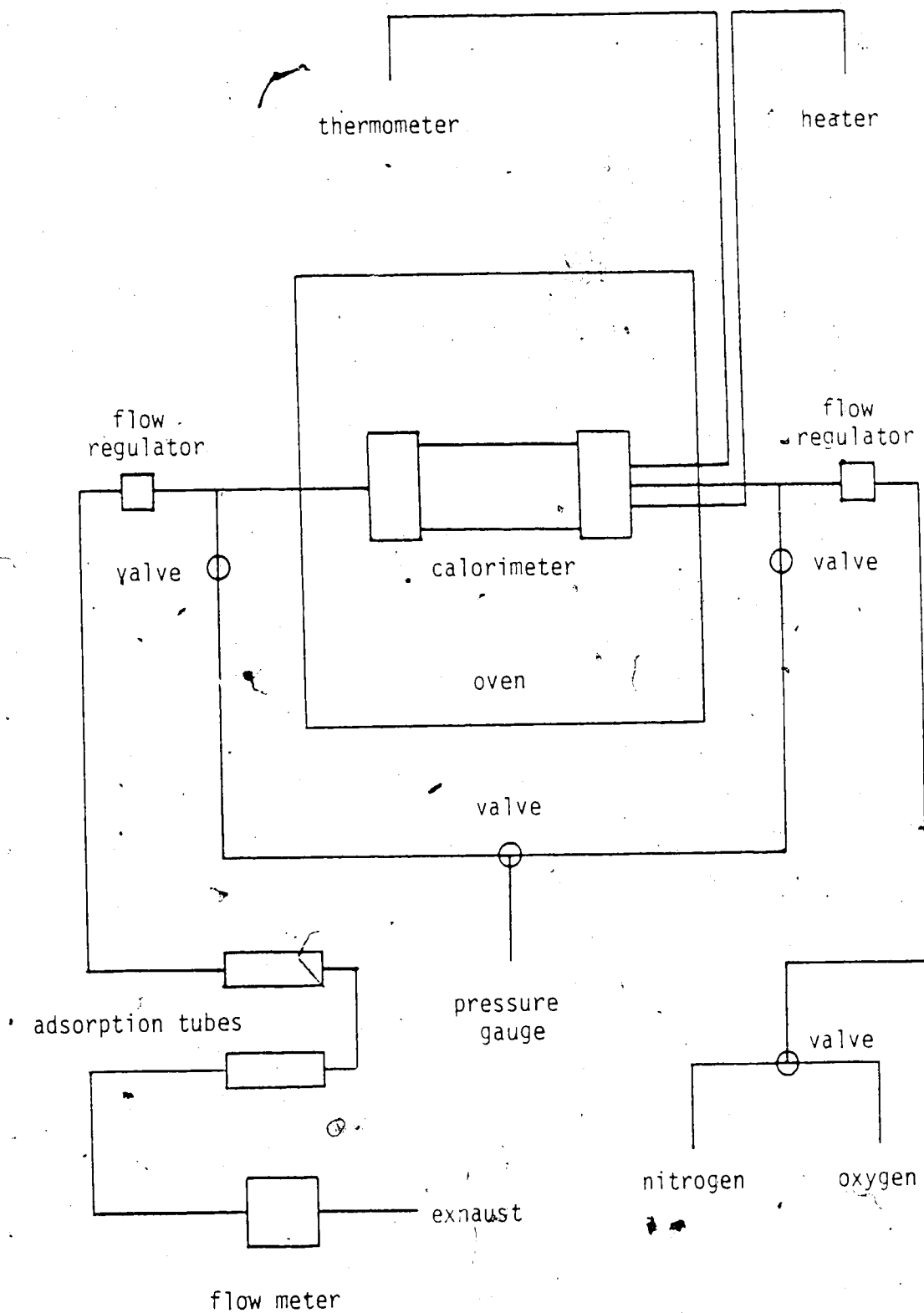


Figure 2-2. Schematic diagram of the calorimetric apparatus for measuring the rate of oxidation of bitumen at low temperatures.

performed calibrations with electrical energy. The following discussion of the calibration procedure refers to Fig. 2-3 and is based on a calibration at 210°C in which 27 mW was supplied for 180 minutes.

Using a suitable electrical circuit (Appendix A), energy is delivered to the calibration heater at a constant and precisely known rate. This power is represented as a function of time by the solid line in Fig. 2-3a. Due to thermal inertia, the power response of the calorimeter is not instantaneous and the temperature-rise response lags the power delivery, as shown by the solid curve in Fig. 2-3b. In addition, there are heat losses. For a particular value of power delivered, the rate of heat losses determines the maximum temperature-rise observable. Thus the power delivered, W , is recovered as the rate of heat gain by the system plus the rate of heat losses to the surroundings.

The rate of heat gain by the system is proportional to the rate of temperature rise relative to the temperature of the surroundings, $(T_{\text{sys}} - T_{\text{surr}})$ or ΔT ,

$$[2-3] \quad W_{\text{gain}} = c \, d\Delta T/dt,$$

where c is the effective heat capacity of the calorimetric system.

Heat loss occurs by conduction, convection, and radiation. Rates of conductive and convective heat losses are obtained from Newton's law of cooling (55):

$$[2-4] \quad W_{\text{cd}} = \kappa_{\text{cd}} \Delta T$$

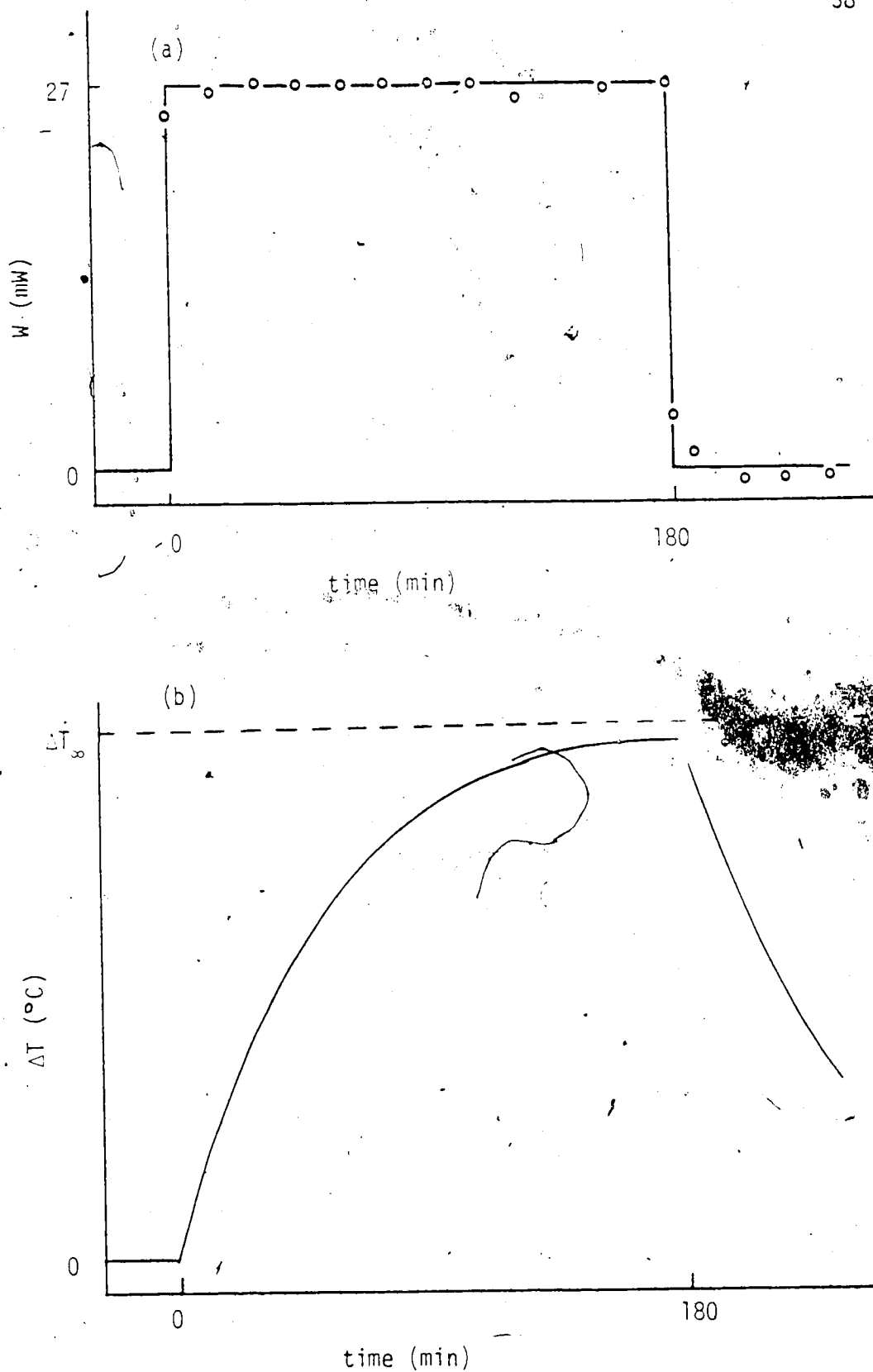


Figure 2-3. Reconstruction of calorimetric records by calibration with electrical energy: (a) time-dependence of power input and power response corrected for thermal lags and heat losses (b) time dependence of temperature rise

$$[2-5] \quad W_{cv} = \kappa_{cv} \Delta T$$

in which κ_{cd} and κ_{cv} are thermal conductances for conduction and convection, respectively. Rate of heat loss by radiation is

$$[2-6] \quad W_{rad} = \sigma(\epsilon_{sys} A_{sys} T_{sys}^4 - \epsilon_{surr} A_{surr} T_{surr}^4)$$

where σ is the Stefan-Boltzmann constant and ϵ_i , A_i , and T_i are the surface emittance, surface area, and surface temperature of the system or surroundings, as indicated by the subscript. Since the geometries of the system and surroundings are fixed relative to one another, eq. [2-6] may be simplified:

$$[2-7] \quad W_{rad} = \kappa_{rad} (T_{sys}^4 - T_{surr}^4)$$

For a small temperature rise of the system relative to the surroundings, the approximation,

$$[2-8] \quad (T_{sys} + T_{surr})/2 = T_{surr}$$

may be introduced (56) and eq. [2-7] becomes

$$[2-9] \quad W_{rad} = \kappa'_{rad} \Delta T$$

$$\text{where } \kappa'_{rad} = 4 \kappa_{rad} T_{surr}^3$$

Combining eq. [2-3]-[2-9] yields the power delivered:

$$[2-10] \quad W = c d\Delta T/dt + \kappa \Delta T$$

where $\kappa = \kappa_{cd} + \kappa_{cv} + \kappa_{rad}$.

The solution to the differential equation [2-10] is

$$[2-11] \quad \Delta T = \Delta T_{\infty} (1 - e^{-(\kappa/c)t})$$

where ΔT_{∞} is the temperature rise approached asymptotically as time elapsed since the onset of heating becomes infinite. Since ΔT_{∞} varies with magnitude of heat losses, it is another quantity to be determined by calibration. Thus there are three calibration constants to be determined using eq. [2-10] and [2-11]: c , κ , and ΔT_{∞} .

Taking the derivative of eq. [2-11] and the logarithm of both sides of the resulting expression gives

$$[2-12] \quad \ln (d\Delta T/dt) = \ln (\kappa/c)\Delta T_{\infty} - (\kappa/c)t.$$

From the record of temperature rise versus time, values of $\ln (d\Delta T/dt)$ at various times are calculated and then plotted versus time, obtaining a line with slope $-\kappa/c$ and intercept $\ln [(\kappa/c)\Delta T_{\infty}]$. Combining the slope and the intercept leads to ΔT_{∞} . Referring to eq. [2-11], when $\Delta T = \Delta T_{\infty}$, $t = \infty$ and $d\Delta T/dt = 0$. Referring to eq. [2-10], then, when $\Delta T = \Delta T_{\infty}$ we have

$$[2-13] \quad W = \kappa \Delta T_{\infty}$$

from which κ may be evaluated since ΔT_{∞} is now known. With the value of κ

known, c may be calculated from the slope of the line represented by eq. [2-12].

The power response of the apparatus, corrected for thermal lags and heat losses as described by eq. [2-10] and calculated using calibration constants obtained in the manner described above, is represented by the open circles in Fig. 2-3a. The close agreement between this corrected response and power input observed in Fig. 2-3a shows that this simple method of analyzing the recorded curves is quite accurate.

We turn now to evaluation of the energetics of the calibration based on the kinetic record. Since the corrected power response of the apparatus is identical to the rate of heat production, the heat, $Q_{1,2}$, developed in any time interval t_1 to t_2 , may be found by integrating eq. [2-14],

$$[2-14], \quad Q_{1,2} = \int_{t_1}^{t_2} W \, dt,$$

in which W is given by eq. [2-10]. The result is

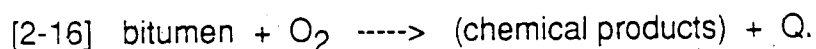
$$[2-15] \quad Q_{1,2} = c \Delta T_{(2-1)} + \kappa \int_{t_1}^{t_2} \Delta T \, dt.$$

The subscript (2-1) on the first term here indicates that the value of ΔT at time t_1 is to be subtracted from the value of ΔT at time t_2 . The cumulative heat developed (time duration t_0 to t) during calibration is plotted as a function of time in Fig. 2-4. Again, close agreement between the corrected response and input functions displayed in this figure shows the high degree of accuracy in the

method described here for analyzing the recorded curves.

Oxidation of Bitumen

By applying eqs. [2-10] and [2-14] to the record of temperature rise versus time obtained experimentally as described above, Fig. 2-5 was constructed to illustrate the time dependence of the kinetics and energetics of the oxidation of our reconstructed tar sand under the experimental conditions cited. The corrected power response shows the expected rapid decrease in the rate of the oxidation as bitumen is consumed in some overall process that we represent here as



The rate of this overall process, expressed in terms of the rate of development of heat, is

$$[2-17] \quad \text{rate} = dQ/dt = W = k(b)^q[P(\text{O}_2)]^r$$

where Q and W are the instantaneous heat and calorific power developed, k is the overall rate constant of process [2-16], b and $P(\text{O}_2)$ are mass percent of bitumen available for oxidation (fuel) and partial pressure of oxygen at time t , and q and r are reaction orders with respect to the reactants, as indicated. The symbol, P , for total pressure is used throughout the following discussions since pure oxygen was used in all experiments.

Because the stoichiometry of process [2-16] is unknown, the ratio of oxidant to fuel is best defined under initial conditions. Therefore, without

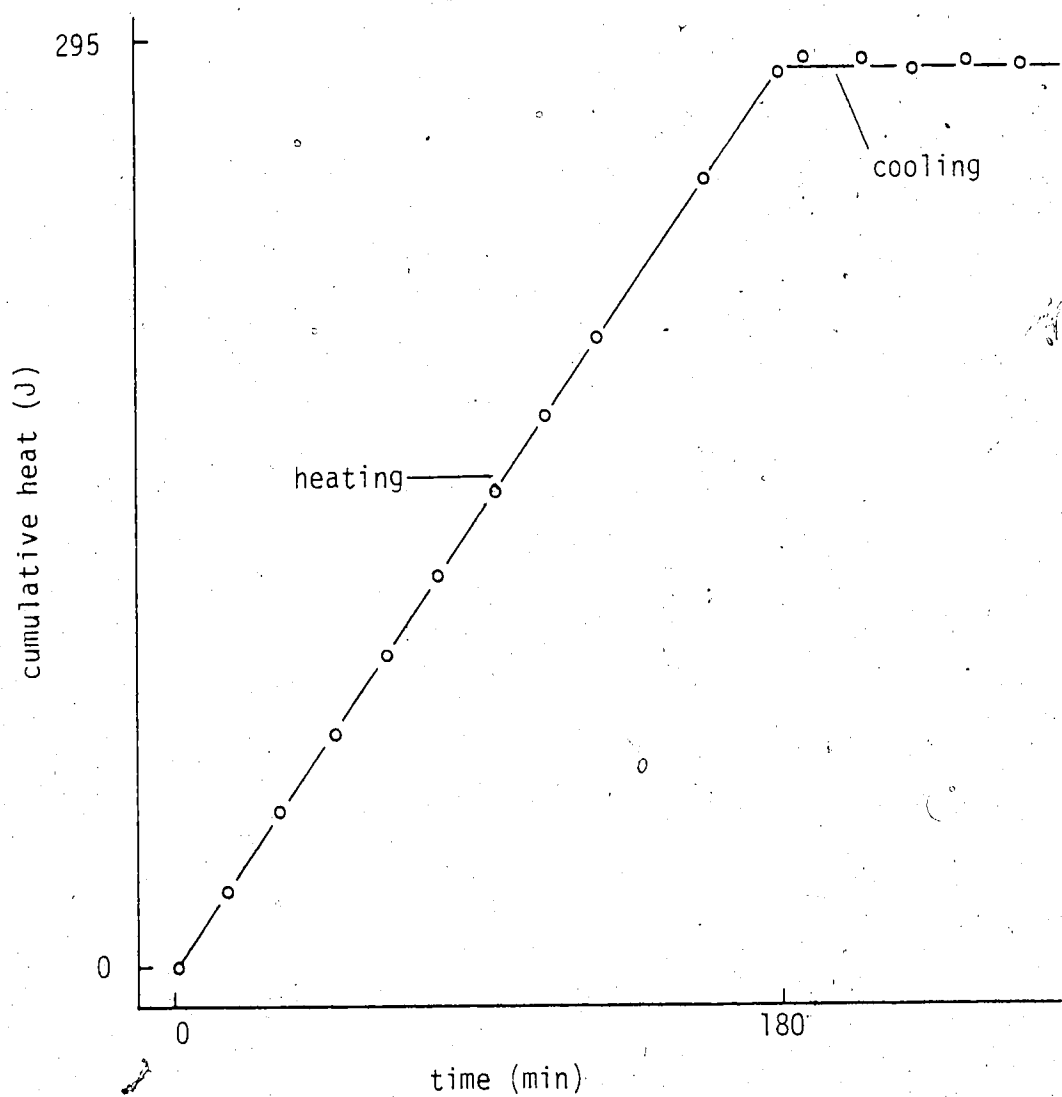


Figure 2-4. Time-dependence of total energy input and energy response corrected for thermal lags and heat losses during calibration.

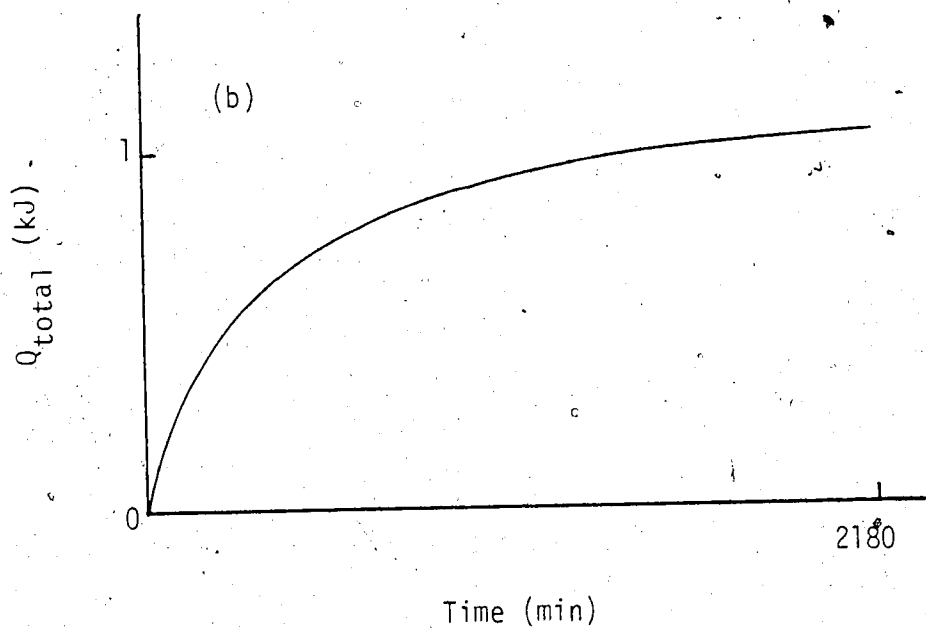
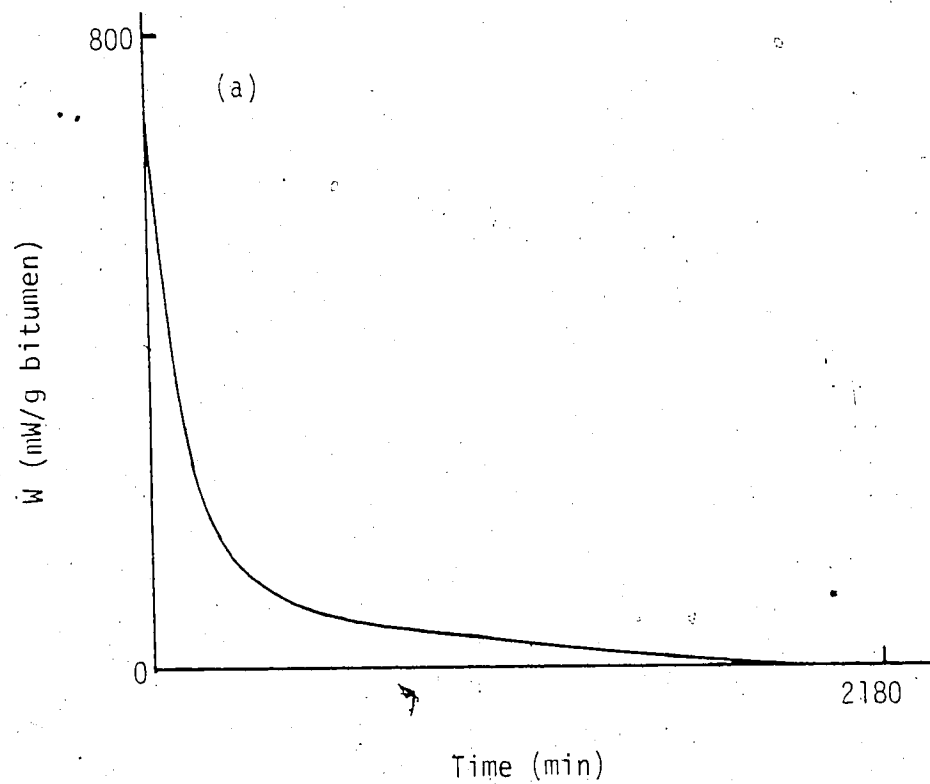


Figure 2-5. Time-dependence of (a) power development and (b) energy release during LTO of bitumen at 210 C and 125 kPa O_2 .

additional assumptions about the mechanism of the process, only the method of initial rates can be applied toward the evaluation of kinetic parameters. Here a number of considerations are relevant. First, the initial concentration of bitumen available for oxidation depends upon whether the reaction with oxygen is homogeneous or heterogeneous. In the former case the bulk mass percent of bitumen is the appropriate compositional variable if the reaction with oxygen occurs in the liquid phase; if the reaction with oxygen occurs in the vapor phase or at the surface of the bitumen, the appropriate compositional variable is some function of the specific surface area of the whole sand. Because of this and other difficulties discussed in the Introduction to this chapter, we have not attempted to determine q , the reaction order with respect to fuel. The effect of fuel concentration on the rate is treated implicitly, by using subsamples of a single tar sand prepared as described previously in performing all calorimetric measurements that are to be correlated with one another. A second consideration arises from the small variation in sample size from one experiment to the next. Since all of the experimental results are to be correlated, the measured rates are normalized by dividing by the mass of bitumen, m_b , present in each sample. Finally, in testing this calorimetric method we choose a narrow range of temperature near the low-temperature limit of the apparatus and assume that the reaction order with respect to oxygen is constant and that the temperature dependence of the rate constant follows the Arrhenius equation [2-2]. On the basis of these considerations, the

normalized initial rate of oxidation, $W_{i(N)}$, may be expressed as

$$[2-18] \quad W_{i(N)} = W_i/m_b = A \exp [-E_a/(RT)] [P(O_2)]^r.$$

The subscript i indicates the initial value of the appropriate quantity.

The initial rate of oxidation is found experimentally by evaluation of the calibration equation [2-10] at $t=0$ ($\Delta T = 0$):

$$[2-19] \quad W_i = c (d\Delta T/dt)_{t=0}.$$

The kinetic parameters A , E_a , and r for the reaction investigated are thus defined by the initial slope of the record of temperature rise versus time.

Results

Measurements were made of the rate of oxidation of bitumen at 155°C and at 210°C for several pressures of pure oxygen between 1 and 3 atmospheres, maintaining a constant flow rate near 13 ml/min. The results are summarized in Table 2-1. Values of the calibration constants used are listed in Table 2-2. The experimental uncertainties in the rate data collected are on the order of 15-20% at 155°C and 7-10% at 210°C. In addition, while the set of measurements at 210°C shows a monotonic increase in initial power with pressure of oxygen, this trend is not apparent at 155°C due to both the small variation in the experimental values of pressure and scatter in the data. For these reasons it is not desirable to fit eq. [2-18] to all of the data in Table 2-1 simultaneously.

In order to evaluate the kinetic parameters for the oxidation reaction, we first linearize eq. [2-18] by taking the logarithm of both sides:

Table 2-1. Rates of production of heat during oxidation of Athabasca bitumen at 155°C and 210°C. Estimated uncertainties in these initial rates are 20% at 155°C and 8% at 210°C.

Temperature (°C)	P(O ₂) (kPa)	flow rate (ml/min)	initial slope (°C/min)×10 ³	initial power (mW/g bit)×10 ⁻²
154.75	141.9	12.5	2.88	1.5
154.70	200.0	12.5	3.48	1.9
156.31	200.4	14.5	2.55	1.4
155.21	250.5	13.5	2.49	1.3
156.05	250.9	12.8	2.93	1.6
155.24	300.9	13.5	3.59	2.0
155.87	302.6	13.5	2.55 ^a	1.4
210.24	107.8	13.0	10.3	6.5
210.23	111.8	13.0	11.5	6.9
210.50	124.3	14.0	11.6	7.3
210.26	124.8	13.5	12.3	8.1
210.06	151.0	12.5	16.4	10.6
210.16	158.0	13.5	16.4	10.5
210.14	210.8	14.0	17.7	11.6
210.21	301.8	13.0	18.6	12.0

Table 2-2. Calibration constants for use in eq. [2-10]

constant	155°C	210°C
c (J/°C)	$342 \pm 3^*$	$427 \pm 31^*$
κ (mW/°C)	111.0	140.9

* average values and one standard deviation based on four measurements

Table 2-3. Kinetic parameters for the LTO of Athabasca bitumen

Source	method	r	E_a (kJ/mol)	Temperature (°C)
Ref. (50)	DTA	$0.98 \pm 0.003^{(a)}$	$64 \pm 3^{(a)}$	175-375
Ref. (43)	$d[m(O_2)]/dt$	$1^{(b)}$	$80 \pm 8^{(c)}$	175-300
		$1^{(b)}$	$67 \pm 6^{(d)}$	175-300
Ref. (42)	$d[m(O_2)]/dt$	variable	variable	22-275
This work	dQ/dt	$0.62 \pm 0.15^{(e)}$	$64 \pm 6^{(e)}$	155-210

(a) Standard deviation of two experiments

(b) Assumed

(c) Single reaction model

(d) Parallel reaction model

(e) r calculated from 210°C data and assumed constant. Average value of $\ln k$ at 155°C was then calculated using this value of r . E_a was evaluated from $\ln k$ at 210°C and 155°C. Later experiments (Ch. 3) confirmed $r=0.6$ at 155°C.

$$[2-20] \quad \ln W_{i(N)} = \ln A - E_a/RT + r \ln [P(O_2)_i].$$

At each temperature eq. [2-20] describes a line with slope r and intercept $\ln k$. This line was then fit to the data collected at 210°C, obtaining values of the reaction order with respect to oxygen, r , and the rate constant, k , at 210°C. This value of r and the data collected at 155°C were then used to calculate an average value of the rate constant at this second temperature. Since the assumption that the reaction orders q and r do not vary over this range of temperature is consistent with the assumption that the rate constant follows the Arrhenius equation, we evaluate an activation energy and a pre-exponential factor, as anticipated in eq. [2-18] and [2-20]. Table 2-3 summarizes the results of this analysis and shows that there is reasonable agreement between the calorimetric results of the present study and the results of two other investigations of low temperature oxidation of Athabasca bitumen.

The need for additional experimentation is underscored by the results of a third study of low temperature oxidation of Athabasca bitumen. Using an integral plug flow reactor under nearly isothermal conditions, Millour *et al.* (42) measured the rate of oxygen consumption in order to follow the progress of LTO at oxygen partial pressures between 200-2000 kPa (total pressure = 4190 kPa) over the temperature range 22-275°C. Their sample was tar sand reconstructed by loading bitumen, which had been extracted with toluene from a core sample, back onto the extracted matrix. Sample composition was 13 mass percent bitumen and included 4 mass percent water. Citing the work of

Adegbesan (57), they state that their flow method does not yield quantitative results below 155°C because of very small oxygen consumption combined with high gas flux needed to ensure kinetic control of the oxidation reaction. At higher temperature they found that the rate of consumption of oxygen did not follow typical Arrhenius behavior and that the rate of reaction was strongly dependent on oxygen partial pressure at low temperature but almost independent of oxygen partial pressure at 175°C.

Yoshiki and Phillips (50) used reconstructed tar sand prepared by loading bitumen onto -60 mesh Norton alundum. Sample composition was 30 mass percent bitumen and sample size was 1 g. In deducing kinetic parameters from DTA thermograms these authors assume that fuel is in excess, i.e., that the reaction order is equal to the reaction order with respect to oxygen. While this is true at the beginning of the temperature scan, it may not be true in the later stages of the scan, where the extent of combustion is appreciable. In view of their quoted precision in temperature ($\pm 0.04^\circ\text{C}$), their reported uncertainty in r is underestimated by at least one order of magnitude. In fact, one standard deviation in a series of five determinations of r at various pressures of air (101-6302 kPa) is larger than 0.01. In this same series of five determinations these authors observed a slight but systematic increase in the value of r with decreasing pressure. At the same time they observed a slight but systematic decrease in the value of the activation energy and a much larger, but also systematic, decrease in the value of the pre-exponential factor. They concluded that at lower pressures combustion reaches completion at higher

temperatures. Although this is equivalent to saying that the LTO is not a single reaction, these authors did not pursue this implication.

Phillips and Hsieh (43) investigated the kinetics of LTO of Athabasca bitumen using an integral plug flow reactor packed with 100 g of whole oil sands and injecting mixtures of oxygen and nitrogen (400 kPa total pressure, 20-90 kPa of oxygen). Observing little or no production of carbon oxides below 250°C and significant production of these gases above this temperature, they proposed a parallel reaction model in which bitumen is simultaneously converted to water and oxygenated hydrocarbons along one path and to CO and CO₂ along a second reaction path. In the single reaction model and in both steps of the parallel reaction model the reaction was assumed to be first order with respect to oxygen concentration and independent of fuel concentration.

In discussing and comparing the four sets of results listed in Table 2-3 there are a number of sources of variation to be considered, including chemical composition of the various samples of Athabasca bitumen, matrix effects, magnitude and range of experimental variables, precision in measurement of the dependent variable, and methods of data analysis. Elemental composition of Athabasca bitumen used in the present work is reported in Chapter 3. Distribution of asphaltenes and maltenes is 16 and 84 mass percent, respectively, and is similar to that of the bitumen used by Millour and coworkers (42). Compositions of bitumens used by Phillips and coworkers (43, 50) were

not reported but are assumed to be similar, so that variation due to composition of bitumen is considered to be minor. Variation due to overall sample composition and matrix effects is more difficult to assess. If kaolinite present in the matrix used by Ref. 42 and 43 catalyzes LTO under the experimental conditions cited, this should be evident in lower values of the activation energy. The activation energy for the single reaction model of Ref. 43, however, is significantly higher than that of Ref. 50 or the present study. The presence of water in the samples of Ref. 42 and 43 is an additional complication, since the role of water in low temperature oxidation is not yet understood. Variation due to the magnitude and range of temperature and pressure is equally difficult to assess. Implicit in the application of the Arrhenius equation to analysis of the kinetics of LTO is the assumption that temperature and pressure are independent and that gases other than oxygen (N_2 , H_2O) are inert diluents that in effect simply alter the distillation characteristics of the bitumen. Since it is probable that some or even all of these experimental variables are coupled, the choice, range, and magnitude of experimental conditions are considered to be major sources of variation in the reported values of kinetic parameters. Because the rate of reaction changes exponentially with temperature, the error in activation energy and reaction order due to precision in measurement of the dependent variable is minor. For the same reason variation due to the use of integrated rate equations as in Ref. 42, 43, and 50 in contrast to the differential method applied in the present work is also minor.

The two points to be noted here are that the oxidation kinetics of Athabasca bitumen are by no means resolved and that, although the kinetic results derived in the present study do not constitute a rigorous test, they do show that the aneroid calorimeter performs as desired.

Before extending measurements to experimental conditions other than those cited in Table 2-1, a preliminary calculation based on the results obtained here was carried out in order to estimate the maximum rate, and hence the maximum temperature, at which reliable measurements can be made with our calorimeter. First we consider that the time at which the maximum rise in temperature occurs depends on the rate of the reaction. The time at which the maximum temperature rise is recorded, however, depends on the response time of the calorimeter, as expressed by the time constant, τ :

$$[2-21] \quad \tau = C/\kappa.$$

In general the limit of precision in a time-dependent measurement is reached when the duration of the process measured is τ/e . This means that the result of a calorimetric measurement of the rate of oxidation is unreliable if the time at which the maximum rise in temperature is recorded is less than τ/e :

$$[2-22] \quad \text{rate}_{\text{max}} = Q_{\text{total}}/(\tau/e).$$

Stated another way, the maximum rate that can be measured reliably is that rate at which the total heat is developed in a time equal to the time constant of the calorimeter:

$$[2-23] \quad Q_{\text{total}} = \int W dt = A \exp[-E_a/(RT)] [P(\text{O}_2)]^r \tau.$$

On the basis of eq. [2-22] the maximum rate measurable at 210°C is about 9000 mW/g, well above the experimental values obtained. Based on data discussed in the next chapter, the maximum rate that can be reliably measured at 320°C is about 50,000 mW/g. From eq. [2-23] the upper temperature limit can be evaluated and is found to be near 300°C. The very small powers developed at 155°C and the resulting low precision indicate that the limit of detection for quantitative application is on the order of 15 mW.

A two-fold variation in flow rate about the value of 14 ml/min used in the test experiments listed in Table 2-1 was found to have no measurable effect on the rate of oxidation. Increase in flow rate, however, increased heat leaks from the calorimeter, while decrease in flow rate led to clogging of the exhaust line with condensed material produced by oxidation and distillation. A flow rate of 13 ml/min has therefore been considered suitable in all subsequent measurements of rates of oxidation.

By amplifying the signal from the thermometer (see Appendix A), greater resolution of the initial slopes of thermograms at 155°C has been obtained (Ch. 3). These later results support the assumption, used in testing the calorimeter as described in this chapter, that r is 0.6 at 155°C as well as at 210°C.

CHAPTER 3

Kinetics and Energetics of Oxidation of Athabasca Bitumen

Introduction

Chapter 2 gave a detailed description of our calorimetric apparatus and method of measuring rates of oxidation. Results of systematic tests of the apparatus at two temperatures were tabulated and analyzed, yielding values of the kinetic parameters for the low temperature oxidation of Athabasca bitumen that are consistent with those of some published studies. The data analysis in all cases assumed that the reaction order with respect to oxygen was constant and that the temperature dependence of the rate constant was consistent with the Arrhenius equation. The requirements implicit in application of the Arrhenius equation to the low temperature oxidation of bitumen and the corresponding experimental difficulties that arise were addressed.

A major conceptual difficulty is that the Arrhenius equation is a good approximation only for processes that involve a single mechanism. Although it has long been recognized that low temperature oxidation of bitumen involves a group of similar reactions in which substances of the same type are produced, it is worth noting that even in the case of homogeneous gas-phase oxidation of simple hydrocarbons at low temperature it is well known that the Arrhenius

equation does not apply over temperature ranges much larger than 50°C , as is evident from changes in product distribution with temperature (58). On this basis Newett and Thornes (59), for example, identified two temperature regimes of slow oxidation of 1:1 mixtures of propane and oxygen. Bradley (60) also noted this behavior in his discussion of the combustion of hydrocarbons. Because of the complex chemical composition and interplay of physical and chemical processes in the low temperature oxidation of a mixture such as bitumen, there is reason to suspect that neither of the two assumptions cited above - that the reaction order with respect to oxygen is constant and that the temperature dependence of the rate constant follows the Arrhenius equation - is valid over the range of temperature spanning the early and late stages of low temperature oxidation.

We therefore wished to test these assumptions in a way that would lead to identification of the correct temperature dependence of the kinetic parameters if the assumptions were in fact found to be unsupported. A suitable way for carrying out this test is to apply a statistical method of process analysis, called the response surface or factorial design method (61). This chapter details the application of this method to the investigation of the rate of the low temperature oxidation of Athabasca bitumen.

Experimental

A new sample of tar sand was prepared as described in Chapter 2, and all experiments were performed using subsamples of this new sand.

A constant gas flow rate of 13.1 ± 0.3 ml/min was maintained for all experiments.

Methods of measurement of initial rates of oxidation and primary data analysis were performed as described in Chapter 2. Using a calibration with electrical energy for each experiment, the records of temperature-rise versus time were transformed into records of calorific power response versus time. Heats developed in time intervals $t=i$ to $t=j$ were obtained by appropriate integration of the function describing power response versus time. Summation of these "interval heats" from $t = 0$ to $t = t(\text{final})$ yielded the total heat developed in each experiment. The data are compiled in Appendix B.

Design of Experiments

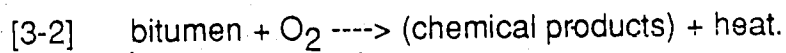
The objective of the response surface method is to identify, by way of efficient experimentation, a model describing the desired response, y , as a function of the factors or independent variables, x_1, x_2, \dots , producing it (61):

$$[3-1] \quad y = b_0 + b_1x_1 + b_2x_2 + \dots$$

In the present case the desired response is the normalized initial rate of heat production and the independent variables of interest are temperature and partial pressure of oxygen. Efficient experimentation is achieved by choosing combinations of values of the independent variables in a statistically prescribed way, leading to unbiased estimates of the model parameters, b_i (61).

During oxidation, bitumen is consumed in some overall process that we

represent as



The rate of this overall process, expressed in terms of the rate of development of heat and applying the method of initial rates, may be written

$$[3-3] \quad W_{i(N)} = k [P(\text{O}_2)_i]^r$$

or equivalently

$$[3-4] \quad \ln W_{i(N)} = \ln k + r \ln [P(\text{O}_2)_i].$$

If r is constant and k varies with temperature as described by the Arrhenius equation, then eq. [3-4] may also be written

$$[3-5] \quad \ln W_{i(N)} = \ln A - E_a/RT + r \ln [P(\text{O}_2)_i].$$

All symbols in eq. [3-3]-[3-5] are as defined previously.

The first-order factorial design model for two independent variables is given by the first three terms of eq. [3-1]:

$$[3-6] \quad y = b_0 + b_1 x_1 + b_2 x_2.$$

Comparison of eq. [3-5] with eq. [3-6] shows that, if both of the assumptions that are to be tested are valid, then the first-order model will fit the experimental data, with identities as follows:

$$[3-7a] \quad \ln W_{i(N)} = y \quad 1/T = x_1 \quad \ln [P(\text{O}_2)_i] = x_2$$

$$[3-7b] \quad \ln A = b_0 \quad E_a/R = -b_1 \quad r = b_2$$

If eqs. [3-6] and [3-7a] do not fit the data, the factorial design may be extended to second-order:

$$[3-8] \quad y = b_0 + b_1x_1 + b_2x_2 + b_3x_1^2 + b_4x_2^2 + b_5x_1x_2$$

We require only five experiments to fit eq. [3-6] and four additional experiments to fit eq. [3-8]. Replicate experiments at the center of the design ($T = 225^\circ\text{C}$, $P(\text{O}_2) = 210 \text{ kPa absolute}$) are included so that we have a measure of experimental error. By comparing the residual variance of the chosen model with variance due to experiment, the significance of the model at any desired confidence level can be tested.

Results and Calculations

Initial rates of heat production

The data in Table 3-1 were collected and analyzed using eqs. [3-6] and [3-7a]. The results obtained are consistent with the previously reported results for measurements at 210°C and 155°C , as can be seen in Table 3-2. The analysis of variance is presented in Table 3-3 and shows that the first-order model is not an adequate description of the data.

The first column in Table 3-3 lists the variations of interest. The third column lists the number of degrees of freedom that belong to each variation. The second column lists for each parameter, b_i , the reduction in the total sum of squares of the residuals (differences between the measured and predicted

Table 3-1. Initial rate of heat production during slow oxidation of bitumen. Data were collected for a first-order factorial design model.

Experiment number	Temperature (°C)	Oxygen pressure (kPa abs)	Initial power (mW/g)x10 ⁻³
1	225.05	210.2	1.91
2	225.42	211.0	1.94
3	225.66	210.8	2.05
4*	154.99	112.1	2.23
5	154.93	397.1	4.50
6	317.32	110.0	22.97
7	317.48	390.9	97.86*

*The estimated maximum reliable rate at this temperature is about 5×10^4 mW/g (see p. 54). The result of experiment 7, however, is well correlated with the result of experiment 6 and with that of the experiment at 317°C and 210 kPa (Table 3-8), both of which are reliable. The result of experiment 7 therefore appears to be accurate.

Table 3-2. Comparison of kinetic parameters derived from first-order response surface measurements with those derived from sets of isothermal measurements at 210°C and 155°C using the Arrhenius equation. The \pm value refers to one standard deviation.

Parameter	Arrhenius equation	Response surface method
$\ln A$	19.5 ± 1.5	19.1 ± 4.3
E_a/R (K)	7700 ± 700	7790 ± 1270
r	0.62 ± 0.15	0.84 ± 0.64
no. of expts.	15	7

Table 3-3. Analysis of variance for a first-order factorial design model, $\ln W_{i(N)} = b_0 + b_1/T + b_2 \ln [P(O_2)_i]$.

Variation	Sum of squares	D.F.	Mean squares	F-test
b_0	13.34	1	13.34	significant
b_1	25.06	1	25.06	significant
b_2	1.14	1	1.14	not significant
variation about zero	472.0	7	67.4	-
regression about zero	470.9	3	157.0	-
lack of fit	1.11	2	0.55	significant
experimental error	0.0025	2	0.0012	-
residual about line	1.11	4	0.28	-

values of y) that would result if b_1 were independently removed from the model.

The next two entries in the second column are the total variance to be explained and the total variance explained by the model. The next two entries are the variance not explained by the model and that portion of the unexplained variance due to experimental error. The last entry is similar to that for the variation due to lack of fit but differs from it by two degrees of freedom, the number of replicate experiments. The fourth column is the mean of the squares of the residuals, the quantities to be used in the various tests of significance. The value for each variation is the sum of squares, in column 2, divided by the number of degrees of freedom. The results of the appropriate tests of significance at the 95% confidence level are listed in the last column.

According to the model, terms in b_0 and b_1 - those describing behavior of the rate constant - are useful in describing the data, but the term in b_2 , which describes the effect of oxygen pressure, is not. Variance due to lack of fit is significantly larger than variance due to experimental error, indicating that the model is not an adequate representation of the data.

The additional data listed in Table 3-4 were then collected and combined with the data of Table 3-1 in a test of the second-order factorial design model represented by eq. [3-8], where the dependent and independent variables are again defined by eq. [3-7a]. All data were weighted equally. The resulting analysis of variance for this model is presented in Table 3-5. In this case, variance due to lack of fit is insignificant relative to variance due to

Table 3-4. Initial rate of heat production during slow oxidation of bitumen. Data were collected for a second-order factorial design model.

Experiment number	Temperature (°C)	Oxygen pressure (kPa abs)	Initial power (mW/g)x10 ⁻²
8	174.00	329.0	6.6
9	173.96	136.3	4.0
10	285.33	332.4	237.6
11	285.49	136.0	134.2

Table 3-5. Analysis of variance for full second-order factorial design model,

$$\ln W_{i(N)} = b_0 + b_1/T + b_2 \ln [P(O_2)_i] + b_3/T^2 + b_4 (\ln [P(O_2)_i])^2 + b_5 (\ln [P(O_2)_i])/T$$

Variation	Sum of squares	D.F.	Mean squares	F-test
b_0	0.0066	1	0.0066	not significant
b_1	0.048	1	0.048	not significant
b_2	0.029	1	0.029	not significant
b_3	0.046	1	0.046	not significant
b_4	0.027	1	0.027	not significant
b_5	0.039	1	0.039	not significant
variation about zero	742.0	11	67.5	-
regression about zero	742.0	6	123.7	-
lack of fit	0.063	3	0.021	not significant
experimental error	0.0025	2	0.0012	-
residual about line	0.063	5	0.013	-

experimental error, but the effect of removing any one of the terms independently of the other four is also insignificant. This circumstance suggests that the model is satisfactory, but overfit, so that at least one of the terms may be omitted.

Because the effect of oxygen pressure on the initial rate of the reaction is much smaller than the effect of temperature, we next tested the second-order model neglecting the term second-order in $\ln [P(O_2)_i]$, with results as summarized in Table 3-6. Again all data were weighted equally. Variance due to lack of fit remained insignificant relative to variance due to experimental error, and each of the terms was found to be useful in representing the data. According to this model, the result of experiment 11 ($T = 285^\circ\text{C}$, $P(O_2) = 136$ kPa) is inconsistent with the results of the other ten experiments and therefore was given a small weight in obtaining the final fit. The variation of the normalized rate of heat production with temperature and oxygen pressure within the limits $155^\circ\text{C} \leq T \leq 320^\circ\text{C}$ and $110 \text{ kPa} \leq P(O_2) \leq 400 \text{ kPa}$ is represented by

$$[3-9] \quad \ln W_{i(N)} = b_0 + (b_1 + b_3/T)(1/T) + (b_2 + b_4/T) \ln [P(O_2)_i].$$

Values of the parameters b_0 through b_4 and their standard deviations at the 95% confidence level are listed in Table 3-7. The largest residual observed is 1.5% in $\ln W_{i(N)}$ at 155°C .

Comparison of eq. [3-9] with eq. [3-4] leads to

Table 3-6. Analysis of variance for second-order factorial design model,
 $\ln W_i(N) = b_0 + b_1/T + b_2 \ln [P(O_2)_i] + b_3/T^2 + b_4 (\ln [P(O_2)_i])/T$.

Variation	Sum of squares	D.F.	Mean squares	F-test
b_0	0.9799	1	0.9799	significant
b_1	1.0042	1	1.0042	significant
b_2	0.3271	1	0.3271	significant
b_3	0.9677	1	0.9677	significant
b_4	0.1637	1	0.1637	significant
variation about zero	651.700	10	65.1700	-
regression about zero	651.681	5	130.336	-
lack of fit	0.0188	3	0.0063	not significant
experimental error	0.0025	2	0.0012	-
residual about line	0.0188	5	0.0038	-

Table 3-7. Model parameters for initial rate of heat production during slow oxidation of bitumen, eq. [3-9]

Parameter	Estimate	$\pm \sigma$ (95% confidence level)
	38.15	7.5
b_1	-320	6200
b_2	2.6844	0.92
b_3	7.2509×10^6	1.44×10^6
b_4	-922.9	440

Table 3-8. Initial rate of heat production during slow oxidation of bitumen. Data were collected for use in isothermal evaluation of rate constants and reaction orders with respect to oxygen pressure for the LTO.

Temp. (°C)	P(O ₂) (kPa)	W _{i(N)} ^(a) (mW/g) $\times 10^{-2}$	W _{i(N)} ^(b) (mW/g) $\times 10^{-2}$	ln k _{ISO} [*]	ln k _{RS}	r _{ISO} [*]	r _{RS}
154.92	210.8	3.2	3.3	2.8	3.0	0.55	0.53
173.95	211.4	5.6	4.8	3.3	2.9	0.56	0.62
285.62	210.4	174.9	153.8	6.4	4.1	0.64	1.03
317.47	209.4	482.1	472.7	4.6	4.8	1.15	1.12

(a) measured value

(b) predicted value

*For each of the four experimental temperatures shown here, one standard deviation (1SD) in ln k based on 3 measurements = 0.02, 0.5, 0.1, 0.03, respectively, and 1SD in r = <0.01, 0.1, 0.02, 0.01, respectively.

$$[3-10] \ln k = b_0 + (b_1 + b_3/T)(1/T)$$

$$[3-11] r = b_2 + b_4/T.$$

Analysis of the initial rates of heat production during low temperature oxidation of bitumen therefore leads to the conclusion that both of the assumptions that were tested are not valid. The logarithm of the rate constant is not linear in $1/T$ as required by the Arrhenius equation, and the reaction order with respect to oxygen increases approximately two-fold over the temperature range from early to late stages of the LTO. The implications of this conclusion and additional supporting evidence will be presented shortly.

Because the dependence of the kinetic parameters on temperature as described by eq. [3-10] and [3-11] is constrained by virtue of the experimental design, these equations, and therefore eq. [3-9] as well, are not expected to be the best representation of the data. In order to assess the reliability of eq. [3-9]-[3-11] and to determine more accurate values for the kinetic parameters, four additional experiments were performed, with conditions and results as described by the first three columns of Table 3-8. Values of the initial power predicted by eq. [3-9] are listed in the fourth column. The largest residual is 2.3% in $\ln W_i(N)$ at 174°C and 211 kPa and is reasonable. The other three experiments are in excellent agreement with the factorial design. Each of these four experiments may be combined with two experiments listed in either Table 3-1 or Table 3-4 to yield four sets of isothermal experiments from which four values of the rate constant and the reaction order with respect to oxygen can be

evaluated. The resulting values are compared with the values predicted by eq. [3-10] and [3-11] in the last four columns of Table 3-8. The values obtained by the response surface method are in agreement with those obtained by the isothermal method within the limits of uncertainty in the former. The largest discrepancy occurs at 285°C, in the region where the reaction order with respect to oxygen is changing rapidly with temperature. A more accurate representation of all of the data, including the result of experiment 11 which did not fit well into the factorial design model, is given by the following empirical equations:

$$[3-12] \quad \ln W_{i(N)} = a_0 + a_1 T + a_2 / (595 - T)^2 + a_3 \ln [P(O_2)_i] + a_4 \ln [P(O_2)_i] / (600 - T)$$

$$[3-13] \quad \ln k = a_0 + a_1 T + a_2 / (595 - T)^2$$

$$[3-14] \quad r = a_3 + a_4 / (600 - T).$$

The largest residual is a few tenths of a percent in $\ln W_{i(N)}$. Values of the coefficients a_0 through a_4 at the 95% confidence level are listed in Table 3-9.

The dependence on temperature of the rate constant and reaction order with respect to oxygen is shown in Figs. 3-1 and 3-2. The rate constant has a maximum near 285°C and is nearly linear with temperature between 155°C and the temperature of the maximum. The reaction order with respect to oxygen is nearly constant at temperatures below 285°C and increases dramatically above 285°C.

Table 3-9. Coefficients for initial rate of heat production, eq. [3-12] rate constant, eq. [3-13], and reaction order with respect to oxygen, eq. [3-14]

Coefficient	Estimate	$\pm \sigma$ (95% confidence level)
a_0	-7.473	1.18
a_1	0.02462	0.0017
a_2	-68.89	18
a_3	0.4517	0.12
a_4	8.4855	2.08

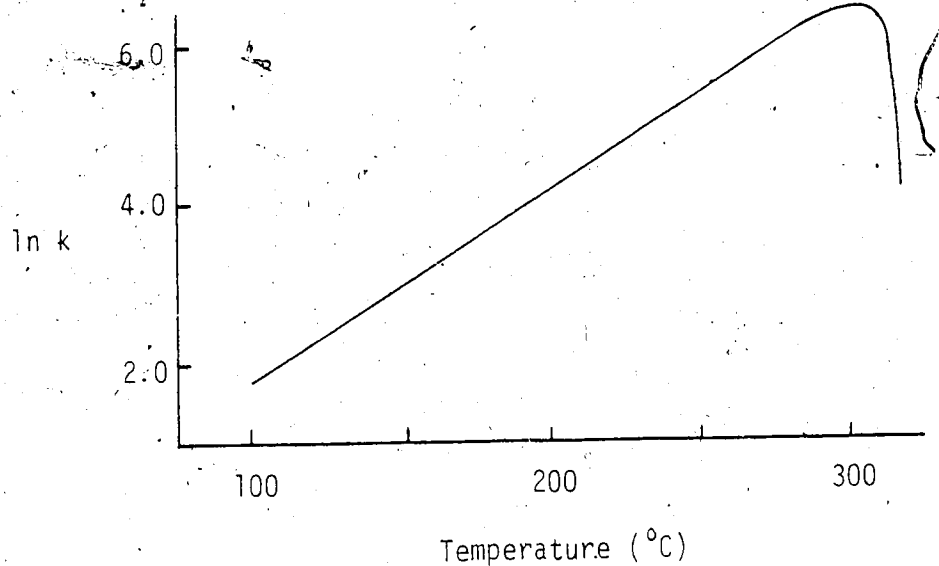


Figure 3-1. Temperature dependence of the global rate constant for oxidation of Athabasca bitumen at low temperatures.

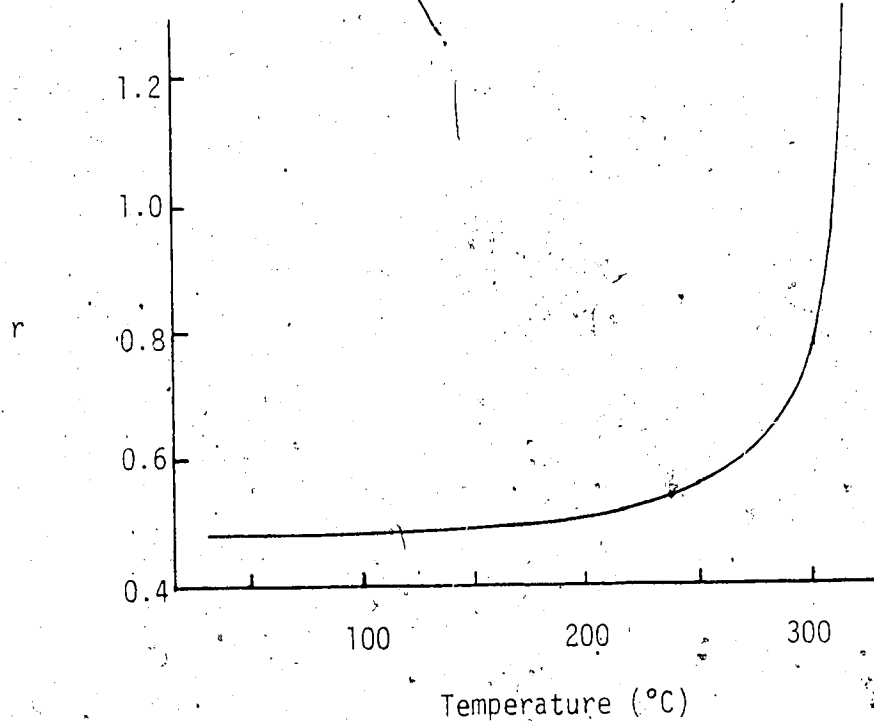


Figure 3-2. Temperature dependence of the reaction order with respect to oxygen for the global oxidation of Athabasca bitumen at low temperatures.

Formation of coke

As stated in the Introduction to this chapter, a change in mechanism with increasing temperature is not unexpected in the case of low temperature oxidation of a complex mixture of hydrocarbons such as bitumen. Such a change will be evident not only in the kinetic parameters but also in the total heat developed in the overall process of combustion, as expressed in eq. [3-2], since this quantity also necessarily reflects the type of reaction occurring. Thus in order to investigate further the implications of the large change in r observed in Table 3-8, additional information was derived from the total heats developed in the kinetic experiments, proceeding as follows.

The records of temperature-rise versus time for most of the experiments cited in Tables 3-1, 3-4, and 3-8, plus an additional experiment at 174°C that was not suitable for use in the analysis of initial rates, were analyzed by methods described in Chapter 2 to obtain the total heats developed. The results, normalized in terms of the original mass of bitumen present in the sample, are summarized in Table 3-10.

Because the system is open there is unavoidable loss of distillable components prior to initiation of the oxidation. If these components would have undergone oxidation, the total heat observed is somewhat too small. Alternatively, distillation may occur also as the result of oxidation, in which case the total heat observed includes both heat released by oxidation and heat absorbed by distillation. Ciajolo and Barbella (49) have shown that paraffinic and aromatic fractions of heavy oils are volatilized at temperatures greater than

Table 3-10. Total heat produced during slow oxidation of bitumen

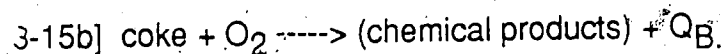
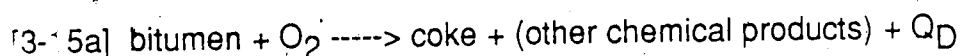
Experiment number	Temperature (°C)	Oxygen pressure (kPa abs)	Sample mass ^(a) (g)	Heat ^(b) (kJ/g bit)
4	154.99	112.1	0.8188	1.6
5	154.93	397.1	0.8262	1.8
9	173.96	136.3	0.8116	1.3
9a	173.85	327.5	0.8145	4.6
8	174.00	329.0	0.7935	4.6
1	225.05	210.2	0.7987	7.4
2	225.42	211.0	0.7985	7.3
3	225.66	210.8	0.8012	7.7
10	285.33	332.4	0.7996	9.5
11	285.49	136.0	0.7993	6.6
6	317.32	110.0	0.8039	7.3
5a	173.95	211.4	0.8322	3.1
10a	285.62	210.4	0.7968	8.1
6a	317.46	209.4	0.8119	8.2

(a) Loading factor is 0.1347 g bitumen per g sample

(b) Precision in measurement of heat increases with temperature and pressure.
Precision is on the order of 15-20% at 155°C, 1-2% at 317°C.

200°C. Oxidation of these fractions in the absence of catalysts occurs only at much higher temperatures (64). Loss of these fractions during thermostating therefore does not affect the heat evolved by oxidation and we may consider that the total heat observed is due almost entirely to oxidation.

The observed normalized variation in total heat from 155°C to 317°C is nearly one order of magnitude, suggesting that the overall process of combustion consists of an initial process releasing little heat at low temperatures and a second process releasing considerably more heat at high temperatures. Since the only products directly accessible in the calorimetric experiments are the total heat and the coked sand itself, for convenience we represent the two processes as one in which coke is produced and one in which coke is consumed:



The total heat, Q , developed in a single calorimetric experiment may then be expressed as the sum of contributions from deposition and burning of coke:

$$[3-16] \quad Q = m_D \Delta H_D + m_B \Delta H_B$$

where subscripts D and B refer to the processes of deposition and burning, respectively, m is mass of coke, and ΔH is enthalpy per gram of coke per gram of bitumen.

Material balance requires that the mass of coke deposited be equal to the mass of coke burned plus the mass of coke remaining as residue, m_R , on the

oxidized tar sand:

$$[3-17] \quad m_D = m_B + m_R.$$

For each of the experiments listed in Table 3-10, the mass of residual coke was determined by ashing the oxidized sample in a muffle furnace at 800°C for two hours.

If we assume that the enthalpies of combustion of bitumen, ΔH_C , and of deposition and burning of coke, ΔH_D and ΔH_B , are constant over the experimental range in temperature, then we may write

$$[3-18] \quad \Delta H_C = \Delta H_D + \Delta H_B.$$

In addition we assume that, of the processes [3-15], only deposition occurs at 155°C. In this case $m_B = 0$, $m_D = m_R$, and eq. [3-16] reduces to

$$[3-19] \quad Q_{155} = m_R \Delta H_D$$

This equation yields ΔH_D since both the total heat developed and the mass of residual coke at 155°C are known. The heat of combustion of bitumen is available from bomb-calorimetric experiments (62), and therefore eq. [3-18] may be combined with eq. [3-19] to yield ΔH_B .

Eq. [3-16] and [3-17] are then combined with the calculated values of ΔH_B to obtain the mass of coke deposited:

$$[3-20] \quad m_D = (Q + m_R \Delta H_B) / \Delta H_C.$$

Table 3-11 summarizes the results of the procedure outlined above. The

amount of coke deposited decreases with increasing temperature and increases with increasing pressure of oxygen. The amount burned also increases with increasing pressure of oxygen and increases with increasing temperature. At 174°C less than 10% of the coke deposited is burned, and therefore the assumption that deposition is the only process of interest at temperatures up to 155°C is a reasonable approximation. Deposition is still the predominant process at 225°C. At 285°C burning of coke becomes more important, but approximately half of the coke deposited remains unburned. At 317°C all coke deposited is burned.

Total heats developed and mass of coke deposited, per gram of bitumen, are represented by the following empirical functions:

$$[3-21] \quad Q = q_0 + q_1/t + P(q_2 + q_3t + q_4t^2)$$

$$[3-22] \quad m_D = m_0 + m_1t + P(m_2 + m_3t + m_4t^2 + m_5t^3)$$

where t is temperature in °C and P is pressure of oxygen in kPa absolute.

Estimated values of the coefficients q_0 - q_4 and m_0 - m_5 at the 95% confidence level are given in Tables 3-12 and 3-13. Both quantities, Q and m_D , are linear in pressure of oxygen. In addition, the pressure dependence of both quantities is weak, so that m_D is nearly linear in temperature and Q is nearly linear in the reciprocal of temperature.

Table 3-11. Coke deposited and burned during slow oxidation of bitumen

Expt. no.	Temperature (°C)	Oxygen pressure (kPa abs)	Residual coke (g/g bit)	Deposited coke ^(a) (g/g bit)	Burned coke ^(a) (g/g bit)
4	154.99	112.1	0.7098	0.7098	0
5	154.93	397.1	0.7494	0.7494	0
9	173.96	136.3	0.6641	0.6592	-(b)
5a	173.95	211.4	0.6700	0.7055	0.0355
9a	173.85	327.5	0.6869	0.7573	0.0704
8	174.00	329.0	0.6929	0.7615	0.0686
1,2,3(c)	225.38	210.7	0.4233	0.5750	0.1517
11	285.49	136.0	0.1541	0.3000	0.1459
10a	285.62	210.4	0.1463	0.3278	0.1815
10	285.33	332.4	0.1443	0.3427	0.1984
6	317.32	110.0	0	0.1699	0.1699
6a	317.47	209.4	0	0.1912	0.1912

(a) Values were calculated using -43 kJ/g of bitumen as the heat of combustion and -2277 J/g of coke deposited as the heat of deposition.

(b) Calculated value is -0.0049 g/g bit. This value represents the order of magnitude of error in the calculation.

(c) Samples from experiments 1, 2, and 3 were pooled.

Table 3-12. Parameters for total heat produced during slow oxidation of bitumen, eq. [3-21]

Parameter	Estimate	$\pm \sigma$ (95% confidence level)
q_0	1.1239×10^4	0.36×10^4
q_1	-1.5571×10^6	0.73×10^6
q_2	-77.526	35
q_3	0.74711	0.31
q_4	-1.5179×10^{-3}	0.65×10^{-3}

Table 3-13. Parameters for deposition of coke, eq. [3-22]

Parameter	Estimate	$\pm \sigma$ (95% confidence level)
m_0	1.1768	0.059
m_1	-3.1944×10^{-3}	0.26×10^{-3}
m_2	-8.4485×10^{-3}	2.9×10^{-3}
m_3	1.0821×10^{-4}	0.39×10^{-4}
m_4	-4.1809×10^{-7}	1.7×10^{-7}
m_5	5.1095×10^{-10}	2.5×10^{-10}

Analysis of cokes and distillates

Elemental compositions of some of the oxidized tar sands produced in the calorimetric experiments were determined by microanalysis in order to confirm the gravimetric results in the case of complete oxidation of bitumen at 317°C and, more importantly, to obtain some information about the effect of temperature on the compositions of the cokes produced and, by inference, on the gross features of the chemical changes occurring in the depositional process. Part (a) of Table 3-14 gives elemental analyses of whole sands before and after oxidation. Part (b) gives the elemental analysis of the support material and elemental compositions of the original bitumen and corresponding cokes produced. No material extractable with toluene or methylene chloride was present in any of the fully oxidized sands.

That complete combustion occurs at 317°C is confirmed by comparison of the last row in part (a) with the first row in part (b). Complete oxidation of sulfur to volatile products occurs between 155°C and 225°C, suggesting that sulfide linkages are broken and sulfur is removed as volatile products of oxidation in the process of deposition. This result is different than that of Maschopedis and Speight (64), who found that sulfur content remained constant at temperatures less than 250°C. The observed increase in oxygen content and decrease in molar ratio of hydrogen to carbon with increasing temperature are consistent with the results of Ref. 64 and with those of others (30,32,41,57,63).

Since carbon is converted to oxide gases in the complete combustion of

Table 3-14. Elemental compositions of tar sands and their constituents before and after low temperature oxidation at 210 kPa abs O₂

(a) weight % composition of whole sands					
Sample	N	C	H	S	coke
unoxidized tar sand	0.13	11.51	1.28	0.98	-
sands oxidized at:					
155°C	0.15	7.57	0.65	0.68	10.12
225°C	0.37	3.76	0.26	0.19	6.18
317°C	0.25	0.13	0.04	0.25	0

(b) weight % composition of tar sand constituents						
Sample	N	C	H	S	O*	molar H/C
chromosorb	0.19	0.21	0.04	0.27	-	-
unoxidized bitumen	nil	84.10	9.25	5.54	1.11	1.32
cokes produced at:						
155°C	nil	72.95	6.07	4.32	16.66	1.0
225°C	3.10	57.63	3.60	nil	35.67	0.77

* oxygen content was calculated by difference

coke, the amount of CO_2 produced in the calorimetric experiments is an additional measure of the extent of oxidation. No CO_2 detectable by ordinary gravimetric techniques was evolved at temperatures below 285°C , in support of the view that the deposition of coke is accompanied by oxidation of functional groups (32,64). This is consistent with the trends in oxygen content and molar H/C as observed above.

Because all coke formed at 317°C is burned, its carbon content can only be estimated. On the basis of the carbon content of the cokes formed at 155°C and the ratio of average mass of coke deposited at 155°C to that deposited at 317°C , we estimate that a single experiment at 317°C would yield only about 55 mg of CO_2 , if the coke formed at 317°C had the same carbon content as the coke formed at 155°C . In view of the change in carbon content with temperature as in Table 3-14(b), the carbon content of cokes formed at 317°C is expected to be much smaller. We actually measured 27.4 mg of CO_2 released by oxidation of 0.8039 g of tar sand at 317°C and 110 kPa absolute of oxygen, leading to a value of 36 wt % as the carbon content of coke formed at 317°C .

As stated earlier, part of the bitumen originally present in the sample is necessarily lost by distillation while the calorimeter is brought to a constant temperature of interest. This loss occurs in any open experimental system such as ours and presumably occurs as well in the *in situ* combustion process in the field. Oxidation produces additional volatile substances. In our apparatus part

of this volatile material condenses in the exhaust gas train and eventually accumulates to the point where it must be removed so as not to interfere with the regulation of gas flow. Although the apparatus was designed specifically to measure the rates of oxidation and is not adapted to quantitative chemical studies of tar sand distillates, some additional useful information may be obtained from an investigation of the distillates collected.

Following each calorimetric experiment the exhaust gas train was flushed first with toluene and then with ethanol. The resulting solutions were combined and the solvents were removed by evaporation. Since the amount of distillate from a single experiment is very small, the distillates from all experiments at the same temperature were pooled to form a composite sample. The amounts of distillate relative to the original mass of bitumen are listed in Table 3-15. No volatile material condensable at room temperature is produced below 155°C. The composite distillate collected at 285°C was separated by chromatography on a column of silica gel, eluting successively with n-pentane, 5% toluene in n-pentane, methylene chloride, and 20% methanol in methylene chloride to yield fractions which we designate as "saturate", "monoaromatic", "polyaromatic", and "polar", respectively. Gas chromatograms of the saturate and monoaromatic fractions were obtained. The FT-IR spectrum of the polar fraction was also obtained. In order to interpret the results of these analyses, bitumen was extracted from the tar sand and similarly fractionated and analyzed. The gravimetric results are reported in Table 3-16. The GC of the saturate fraction showed the same features as that of the saturate fraction of the

Table 3-15. Tar sand distillates collected at room temperature during low temperature oxidation of bitumen

Temperature (°C)	g distillate/g bitumen
155	0
174	0.15
285	1.07
317	0.56

Table 3-16. Fractionation of original bitumen and produced oil, expressed as weight %

Fraction	Original bitumen ^(a)	Oil produced at 285°C ^(b)
saturate	27.6	51.0
monoaromatic	18.8	17.7
polyaromatic	31.9	17.5
polar	21.7	13.8

(a) 215.0 mg analyzed

(b) 231.0 mg analyzed

original bitumen. Some substances having up to 34 carbon atoms were observed to have distilled out of the oxidized tar sand. No carbonyl or carboxyl groups were observed in the original bitumen, but both were present in the polar fraction of the distillate. Sulfoxide was also present in this fraction of the distillate.

Black particles insoluble in both toluene and ethanol were present in all of the distillates. Particulate matter has been observed by others in the products of low temperature oxidation of bitumen in closed systems and is thought to form by aggregation of polar by-products (49,63-65). The presence of these particles in the distillates indicates that the particles are formed from volatile products and therefore that their presence should be anticipated in oils produced by *in situ* combustion. Because of the polar nature of these particles, it is possible that they will be adsorbed onto the reservoir material and by this means reduce permeability of the tar sand ahead of the combustion front.

Discussion

The combined analyses of cokes and distillates have shown that the decrease in conversion of carbon to coke from 63% at 155°C to less than 8% at 317°C is accompanied by a maximum in the yield of produced oil at 285°C. Along with the kinetic results this situation supports the conclusion that the oxidation processes occurring at temperatures up to 285°C are of a fundamentally different type than those occurring above 285°C and that these

processes may be presented in terms of reactions leading to the formation of coke and other generated hydrocarbons at low temperatures and reactions leading to the burning of coke and other hydrocarbons at high temperatures. It is now possible to transform the mathematical model of the overall rate of oxidation expressed in the empirical equations [3-12]-[3-14] into a chemical model based on the two processes recognized.

Let us consider again that the total heat released in the overall oxidation is the sum of contributions from processes of deposition and burning of coke as expressed in eq. [3-16]. The derivative of this equation with respect to time gives the relationship between the measured overall rate of oxidation, $W_{(N)}$, and the rates of deposition and burning of coke, W_D and W_B , respectively:

$$[3-23] \quad W_{(N)} = W_D + W_B$$

where $W_{(N)} = dQ/dt$

$$W_D = \Delta H_D (dm_D/dt)$$

$$W_B = \Delta H_B (dm_B/dt)$$

At 155°C only deposition occurs and therefore $m_B = 0$, $dm_B/dt = 0$, and $W_D = W_{(N)}$. The reaction order with respect to oxygen pressure at this temperature was found to be 0.55 and is now taken to be the reaction order with respect to oxygen pressure for the deposition reaction. Combining the rate data for 155°C with those for 174°C, where deposition still strongly predominates, allows

evaluation of the activation energy and pre-exponential factor for the deposition reaction.

This information may then be used to calculate the rate of deposition at 225, 285, and 317°C at each of the experimental pressures. Combining these values with the measured values of the overall rate of oxidation yields the rate of the reaction in which coke is burned, by way of eq. [3-23]. Here it is assumed that the reaction order with respect to oxygen pressure is the maximum value observed, i.e., $r_B = 1.15$. Combining the resulting values of W_B at 225, 285, and 317°C allows evaluation of the activation energy and pre-exponential factor for the combustion reaction.

The resulting chemical model is represented by the following equations:

$$[3-24] \quad \ln W_D = \ln A_D - E_{a(D)}/RT + r_D \ln [P(O_2)]$$

$$[3-25] \quad \ln W_B = \ln A_B - E_{a(B)}/RT + r_B \ln [P(O_2)]$$

$$\text{where } \ln A_D = 14.8$$

$$\ln A_B = 31.6$$

$$E_{a(D)}/R = 5147 \text{ K}$$

$$E_{a(B)}/R = 15921 \text{ K}$$

$$r_D = 0.55$$

$$r_B = 1.15$$

Since the uncertainty in values of activation energies is on the order of 10%, the value of the activation energy for the combustion reaction found in this work, 132 kJ/mol, is in good agreement with the value of 145 kJ/mol obtained by Phillips and Hsieh (43) and is expected since the value of $r = 1$ assumed by these authors is very near the value $r = 1.15$ obtained here. The values of

activation energy for the depositional reaction, 43 kJ/mol in the present work and 67 kJ/mol in Ref. 43, are significantly different. This is also expected on the basis of the difference in the values of $r = 1$ assumed in Ref. 43 and $r = 0.55$ obtained in the present work. Hayashifani (66), Haidar (67), and Yoshiki and Phillips (50) report values of approximately 200 kJ/mol for the activation energy for the formation of coke by thermal cracking of Athabasca bitumen. The value of the activation energy for the deposition of coke by low temperature oxidation found in this work is considerably lower, indicating that low temperature oxidation promotes deposition of coke and may lead to reduced recovery in the *in situ* combustion process.

One of the more obvious implications of the model represented by eq. [3-24] and [3-25] is that the maximum rate at which coke can be burned is the rate at which it is produced. By combining the two equations it can be shown that the temperature of the steady state,

$$dm_D/dt = dm_B/dt,$$

varies inversely with $P[O_2]^{0.6}$. This temperature decreases from 390°C at $P[O_2] = 50$ kPa to about 335°C at 600 kPa. We can therefore account for the shift, observed in many DTA experiments, of peak combustion temperature towards lower temperature with increasing oxygen partial pressure.

Finally, we consider the interpretation of the results obtained in this study in relation to field process variables in the enhanced recovery of bitumen and heavy oils by *in situ* combustion. Among the factors to be optimized are the

cost in air compression, the desirable peak temperature, recovery efficiency (ratio of mass of hydrocarbons recovered to mass of bitumen originally in place), and fuel conversion sufficient to sustain combustion. Because the amount of bitumen consumed as fuel is not directly accessible in the calorimetric experiments, assessment of these factors requires complementary chemical investigations that provide this information. One important field process variable that can be calculated using the kinetic data obtained in this study is the ignition delay, or the time required to bring a unit mass (or volume) of formation from ambient to combustion temperatures, near 300°C. Since depositional processes predominate in this temperature range, the ignition delay is approximately equivalent to the time required to complete the depositional phase of the global oxidation reaction. In the absence of external heat sources this time may be estimated in the following way.

Assuming adiabatic reservoir conditions, the heat available for raising the temperature of the reservoir in a time element, dt , is the heat released per unit time per unit mass of bitumen, W :

$$[3-26] \quad \text{heat produced} = Wdt = k [P(O_2)]^r dt.$$

Part of this heat will be needed to vaporize the water in the tar sand and the rest will be available for heating the reservoir:

$$[3-27] \quad \text{heat absorbed} = f_w \Delta H_v / f_b + (c_{ts} / f_b) dT$$

where f_w and f_b are the fractions of water and bitumen in the tar sand, respectively, ΔH_v is the heat of vaporization of water, and c_{ts} is the specific heat

capacity of the tar sand. Equating [3-26] and [3-27], separating variables, and integrating yields

$$[3-28] \quad t = f_w \Delta H_v / (f_b k [P(O_2)]^r) + \int c_{ts} / (f_b k [P(O_2)]^r) dT.$$

As can be seen from Fig. 3-2, r is nearly independent of temperature below the combustion temperature and for convenience may be held constant in this calculation. We choose $r = 0.48$, the extrapolated value at an initial reservoir temperature of 300 K. This value is in reasonable agreement with a few values published by others (39,40,68). The first term in eq. [3-28] is evaluated at the temperature of the transition of water from liquid to vapor. Fig. 3-1 shows that the temperature dependence of the rate constant, k , below the temperature of the transition from depositional to combustion processes is given by the first two terms of eq. [3-13]. The second term in eq. [3-28] becomes

$$1/(f_b [P(O_2)]^{0.48}) \int_{300}^{600} (c_{ts}/k) dT.$$

For convenience an upper limit of $T = 600$ K is chosen. Because of the exponential variation in k with temperature, the actual value of the upper limit contributes negligibly to the value of the integral and hence is arbitrary provided it is far above the initial temperature of the reservoir. The specific heat capacity of the reservoir can be represented as an additive function of the specific heat capacities of the reservoir components as shown by Cassis *et al.*

(54):

$$[3-29] \quad c_{ts} = f_b c_b + f_{cs} c_{cs} + f_{fs} c_{fs} + f_w c_w$$

where subscripts cs and fs refer to coarse and fine solids, respectively, f_i is the fraction of component i , and c_i is the corresponding specific heat capacity.

Using heat capacity data from Ref. 54 for Athabasca tar sand and assuming typical fractional mass compositions of 0.11 bitumen, 0.69 coarse solids, 0.16 fine solids, and 0.04 water, eq. [3-28,29] were combined to yield the simple expression

$$[3-30]. \quad t = 1256/[P(O_2)]^{0.48}$$

where $P(O_2)$ is pressure of oxygen in kPa absolute and t is time in days required for completion of the depositional phase of the LTO process per metric ton of tar sand. This relationship is shown in Fig. 3-3. Beyond a few hundred kPa of oxygen, the reduction in time of deposition with increasing pressure of oxygen becomes quite small.

The procedure outlined here may similarly be applied to other tar sands for which the composition, as specified in eq. [3-29], constituent specific heat capacities, and kinetic parameters are known. It is important to note that the form of eq. [3-30] is completely general. The values of the constant term in the numerator and the reaction order with respect to oxygen, r , in the denominator are expected to vary only slightly from one tar sand to another.

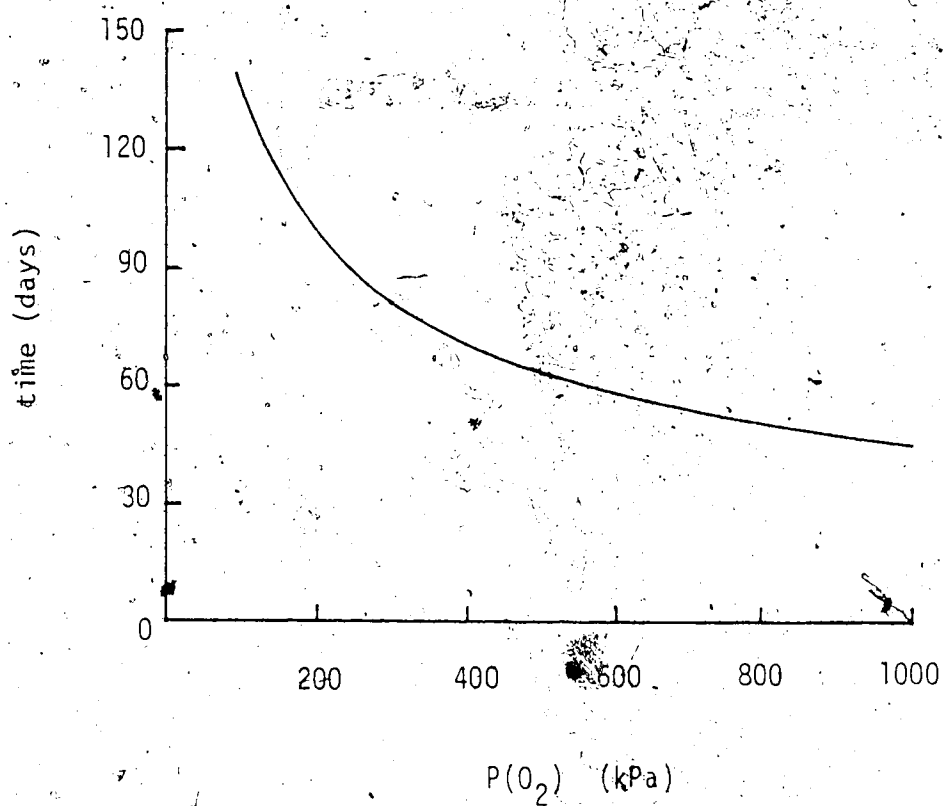


Figure 3-3. Effect of oxygen partial pressure on the time of completion of depositional reactions during LTO of Athabasca bitumen. Time is per metric ton of tar sand.

References

1. D. D. Wagman, W. H. Evans, V. B. Parker, R. H. Schumm, I. Halow, S. M. Bailey, K. L. Churney, and R. L. Nuttall. J. Phys. Chem. Ref. Data **11**, Suppl. 2 (1982).
2. K. S. Pitzer. J. Phys. Chem. **77**, 268 (1973).
3. H. C. Helgeson and D. H. Kirkham. Am. J. Sci. **276**, 97 (1976).
4. H. C. Helgeson, D. H. Kirkham, and G. C. Flowers. Am. J. Sci. **281**, 1249 (1981).
5. D. Smith-Magowan and R. H. Wood. J. Chem. Thermodyn. **13**, 1047 (1981).
6. P. S. Z. Rogers and K. S. Pitzer. J. Phys. Chem. **85**, 2386 (1981).
7. J. A. Barbero, L. G. Hepler, K. G. McCurdy, and P. R. Tremaine. Can. J. Chem. **61**, 2509 (1983).
8. P. R. Tremaine, K. Sway, and J. A. Barbero. J. Solution Chem. In press.
9. J. P. Hershey, S. Sotolongo, and F. J. Millero. J. Solution Chem. **12**, 233 (1983).
10. J. P. Hershey, R. Damesceno, and F. J. Millero. J. Solution Chem. **13**, 825 (1984).
11. J. K. Hovey and P. R. Tremaine. Géochim. et Cosmochim. Acta **50**, 453 (1986).
12. International Critical Tables, Vol. 3. McGraw-Hill Book Co., Inc., New York. 1928. p.70 and p.97.

13. L. H. Milligan. J. Am. Chem. Soc. **44**, 567 (1922).
14. K. Fajans and O. Johnson. J. Am. Chem. Soc. **64**, 668 (1942).
15. F. J. Millero. *In* Water and aqueous solutions: structure, thermodynamics, and transport processes. Edited by R. A. Horne. Wiley-Interscience, New York, 1972. [Chapt. 13]
16. P. Picker, E. Tremblay, and C. Colbourne. J. Solution Chem. **3**, 337 (1974).
17. G. S. Kell. *In* Water—a comprehensive treatise. Vol 2. Edited by F. Franks. Plenum, New York, 1972.
18. J. L. Fortier, P.-A. Leduc, and J. E. Desnoyers. J. Solution Chem. **3**, 323 (1974).
19. L. Haar, J. Gallagher, and G. S. Kell. NBS/NRC Steam Tables. Hemisphere, New York, 1984.
20. P. S. Z. Rogers and K. S. Pitzer. J. Phys. Chem. Ref. Data **11**, 15 (1982).
21. F. J. Millero. Chem. Rev. **71**, 147 (1971).
22. T. F. Young and M. B. Smith. J. Phys. Chem. **58**, 716 (1954).
23. G. Akerlof and J. Teare. J. Am. Chem. Soc. **60**, 1226 (1938).
24. K. S. Pitzer and J. J. Kim. J. Am. Chem. Soc. **96**, 5701 (1974).
25. K. S. Pitzer. J. Solution Chem. **4**, 249 (1975).
26. D. J. Bradley and K. S. Pitzer. J. Phys. Chem. **83**, 1599 (1979).
27. O. Enea, P. P. Singh, E. M. Woolley, K. G. McCurdy, and L. C. Hepler. J. Chem. Thermodyn. **9**, 731 (1977).
28. P. S. Z. Rogers. Thermodynamics of Geothermal Fluids. Ph.D. thesis, Earth Sciences Division, U. C. Berkeley, LBL-12386, 1981. Chapt. 2,3.

29. (a) K. S. Pitzer, J. R. Peterson, and L. F. Silvester. *J. Solution Chem.* **7**, 45 (1978).
(b) W. M. Gildseth, A. Habenschuss, and F. H. Spedding. *J. Chem. Eng. Data* **20**, 292 (1975).
(c) A. Habenschuss and F. H. Spedding. *J. Chem. Eng. Data* **21**, 95 (1976).
30. H. J. Tadema. *Proc., Fifth World Petroleum Congress, New York, 1959*. Section II, Paper 22, 279.
31. F. W. Smith and T. K. Perkins, Jr. *J. Can. Pet. Technol.* **12**, 44 (1973).
32. J. Burger and B. Sahuquet. *Rev. Inst. Fr. Pet.* **32**, 141 (1977).
33. K. N. Jha. "Application of Thermal Analytical Techniques to Enhanced Oil Recovery", presented at the ACS meeting in Washington, D. C., Aug. 28-Sept. 2, 1983. p. 1176.
34. K. N. Jha and B. Verkočzy. SPE/DOE 12677, Fourth Symposium on Enhanced Oil Recovery, Tulsa, OK, Apr. 15-18, 1984. p. 459.
35. R. Kharrat, S. Vossoughi. *J. Pet. Technol.* **37**, 1441 (1985).
36. S. Vossoughi. *Thermochim. Acta* **126**, 63 (1986).
37. J. D. Alexander, W. L. Martin, and J. N. Dew. *J. Pet. Technol.* **14**, 1154 (1962).
38. J. G. Burger and B. C. Sahuquet. *J. Pet. Eng. J.* **12**, 410 (1972).
39. M. K. Dabbous and B. F. Fulton. *J. Pet. Eng. J.* **14**, 253 (1974).
40. K. J. Tadema and J. Weijdemans. *Oil and Gas J.* **68**, 77 (1970).

41. R. Z. Fassihi, W. E. Brigham, and H. J. Ramey, Jr. Soc. Pet. Eng. J. **24**, 399 (1984), Soc. Pet. Eng. J. **24**, 408 (1984).
42. J. P. Millour, R. G. Moore, D. W. Bennion, M. G. Ursepack, and D. N. Gie. "An Expanded Compositional Model for Low Temperature Oxidation of Athabasca Bitumen", Paper no. 86-32-41, Petroleum Society of CIM, June 8-11, 1986.
43. C. R. Phillips and I. G. Hsieh. Fuel **64**, 985 (1985).
44. J. H. Bae. "Characteristics of Crude Oil for Fireflooding Using Thermal Analysis Methods", SPE 6173, 51st Annual Fall Tech. Conf. and Exhibition of the Soc. of Pet. Eng. of AIME, New Orleans, LA, Oct. 3-6, 1976.
45. S. Vossoughi and G. P. Willhite. "Effect of Clay on Crude Oil in In-Situ Combustion Process", SPE 10320, 56th Annual Fall Tech. Conf. and Exhibition of the Soc. of Pet. Eng. of AIME, San Antonio, TX, Oct. 5-7, 1981.
46. S. Vossoughi and G. P. Willhite. "Effect of Sand Grain Specific Surface Area on the Performance of the Tube In-Situ Combustion Process", SPE 11072, 57th Annual Fall Tech. Conf. and Exhibition of the Soc. of Pet. Eng. of AIME, New Orleans, LA, Sept. 26-29, 1982.
47. S. Vossoughi and G. P. Willhite. SPE 11073, 57th Annual Fall Tech. Conf. and Exhibition of the Soc. of Pet. Eng. of AIME, New Orleans, LA, Sept. 26-29, 1982.

48. S. Vossoughi, G. Willhite, Y. El Shoubary, and G. Bartlett. *J. Therm. Anal.* **27**, 17 (1983).
49. A. Ciajolo and R. Barbella. *Fuel* **63**, 657 (1984).
50. K. S. Yoshiki and C. R. Phillips. *Fuel* **64**, 1591 (1985).
51. O. Drici and S. Vossoughi. *J. Pet. Technol.* **37**, 731 (1985).
52. S. Vossoughi, G. W. Bartlett, and G. P. Willhite. *Soc. Pet. Eng. J.* **25**, 656 (1985).
53. B. Verkoczy and K. N. Jha. *J. Can. Pet. Technol.* **25**, 47 (1986).
54. R. Cassis, N. Fuller, L. G. Hepler, R. J. C. McLean, A. Skauge, N. S. Srinivasan, and H.-K. Yan. *AOSTRA J. of Res.* **1**, 163 (1985).
55. F. Kreith. *Principles of Heat Transfer*, 3rd ed. Harper and Row, New York. 1973. Chapt. 1.
56. J. A. Adams and D. F. Rogers. *Computer-Aided Heat Transfer Analysis*. McGraw-Hill, Inc., New York. 1973. p. 29.
57. K. O. Adegbesan. *Kinetic Study of Low Temperature Oxidation of Athabasca Bitumen*. Ph.D. thesis, The University of Calgary, Calgary, Alberta, 1982.
58. G. J. Minkoff and C. F. H. Tipper. *Chemistry of Combustion Reactions*, London, Butterworths, 1962. Chapt. 4, 5.
59. D. M. Newitt and L. S. Thorne. *J. Chem. Soc.*, 1657 (1937).
60. J. N. Bradley. *Flame and Combustion Phenomena*. Methuen and Co., Ltd., London, 1969. Chapt. 6, 8.

61. D. M. Himmelblau. Process Analysis by Statistical Methods. John Wiley and Sons, Inc., N. Y., 1970. Chapt. 8.
62. H.-K. Yan and L. G. Hepler. Personal communication.
63. W. L. Martin, J. D. Alexander, and J. N. Dew. Trans. Am. Inst. Min. Metall. Pet. Eng. **213**, 28 (1958).
64. S. E. Moschopedis and J. G. Speight. Fuel **54**, 210 (1975).
65. N. A. Nouredin, F. M. Mourits, D. G. Lee, and K. N. Jha. AOSTRA J. of Res., in press.
66. M. Hayashitani, D. W. Bennion, J. K. Donnelly, and R. G. Moore. "Thermal Cracking of Athabasca Bitumen", The Oil Sands of Canada - Venezuela Symposium; CIM Special Publication 17, 233 (1977).
67. N. I. Haidar. M. A. Sc. thesis, The University of Toronto, Toronto, Ontario, 1982.
68. J. Burger. Soc. Pet. Eng. J. **16**, 73 (1976).
69. J. Coops, R. S. Jessup, and K. van Nes. In Experimental Thermochemistry. Edited by F. D. Rossini. Interscience Publishers, Inc., New York. 1956. Chapt. 3.

Appendix A. Measurement of power input to the calibration heater and of temperature versus time

Fig. A-1 shows the circuit diagram and elements used to measure power input to the calibration heater. This power, W_h , is the product of the current through the heater, I_h , and the voltage across the heater, V_h :

$$[A-1] \quad W_h = I_h V_h$$

The total current that is supplied by a constant 30 V power supply, PS, is regulated by way of a variable decade resistor, R_{V1} , and measured as the ratio of voltage to resistance of a standard resistor of low resistance, R_{S1} , in series with R_{V1} :

$$[A-2] \quad I = V_{S1}/R_{S1}$$

A large series standard resistance, $R_{S2} + R_{S3}$, in parallel with the heater is used to measure I_h and V_h . These quantities are given by the following equations:

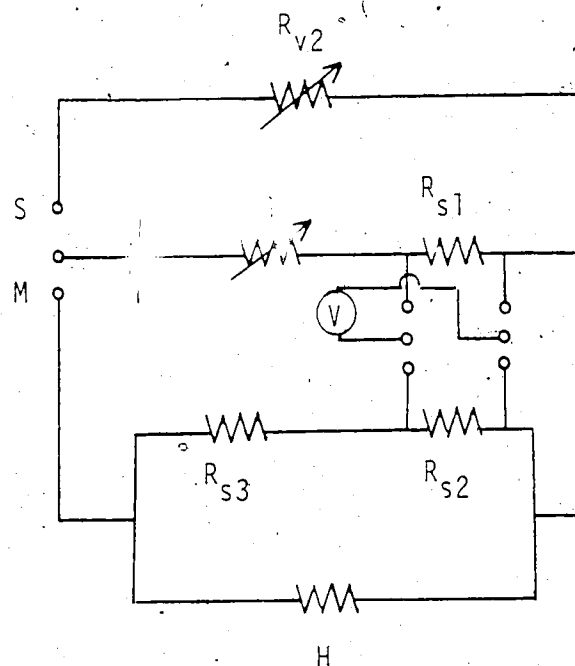
$$[A-3] \quad I_h = I - V_{S2}/R_{S2}$$

$$[A-4] \quad V_h = (I - I_h)(R_{S2} + R_{S3})$$

Since the resistances of the standards are known independently, measurement of the voltages across R_{S1} and R_{S2} , both of which are on the order of a few mV, allows calculation of the calibrating power by way of equations [A-1]-[A-4].

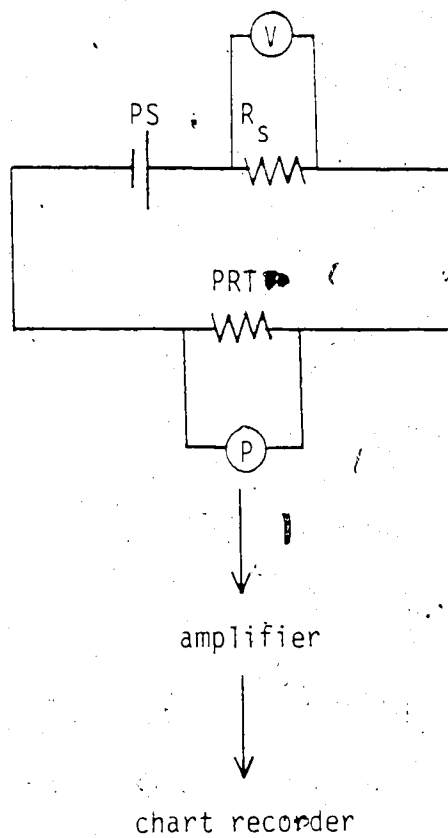
Using a design similar to one described by Coops *et al.* (69), a stabilizing circuit is established with a variable decade resistor, R_{V2} , adjusted to the approximate resistance of the heater. With the single pole switch in the S-position, the power supply is allowed to run until self-heating effects in R_{V1} are absent. The switch is then thrown to the M-position and a stop-watch is started. The position on the strip chart corresponding to this time is marked and V_{S1} and V_{S2} are recorded. The calibration is continued for 2-3 hr, with time and voltages recorded every or three times during this period to check the constancy of both the power delivery and the chart speed.

Fig. A-2 shows the circuit diagram and elements used to measure temperature rise versus time. The current supplied by a constant 20 V power supply, PS, is regulated at 2.000 ± 0.005 mA by a large standard resistance, R_S , in series with the platinum resistance thermometer, PRT. At the beginning of a calibration or an experiment the voltage across the PRT is offset by a potentiometer, P. The output of the galvanometer is fed through an amplifier to the strip-chart recorder. The baseline voltage of the chart thus corresponds to the voltage of the thermometer at the equilibrium temperature, $T_{sys} = T_{surr}$, and is identified through the calibration constants of the thermometer combined with measurement of the voltage across the thermometer leads. Similar measurement of temperature during calibration of the calorimetric system or during an experiment allows calibration of the chart.



PS	power supply
R_{v1}, R_{v2}	variable resistances
R_{s1}	standard resistance, 0.1Ω
R_{s2}	standard resistance, 100Ω
R_{s3}	standard resistance, $100,000\Omega$
V	voltmeter
S	stabilizing circuit
M	measuring circuit
H	heater

Figure A-1. Circuit diagram for measuring power input to the calibration heater.



PS power supply

R_s standard resistance, 10,000 Ω

PRT platinum resistance thermometer

P potentiometer

V voltmeter

Figure A-2. Circuit diagram for measuring temperature rise.

Appendix B. Temperature versus time data for thermokinetic investigation of the low temperature oxidation of Athabasca bitumen

Individual experiments are identified by temperature, absolute pressure of oxygen, and sample mass. Loading factor is 0.1347 g bitumen/g sample. Symbols are defined as follows:

T	temperature
$P(O_2)$	absolute pressure of oxygen
m_s	sample mass
κ	heat transfer coefficient
c	heat capacity of calorimetric system
s	chart speed
θ	chart sensitivity
ΔT_{\max}	maximum rise in temperature
t	time
ΔT	temperature rise due to oxidation
$d\Delta T/dt$	slope of temperature vs. time curve
W	calorific power developed
$Q_{i,j}$	heat developed in time interval $t=i$ to $t=j$
Q	heat developed in time interval $t=0$ to t

Equations used to calculate power, W , interval heat, $Q_{i,j}$, and total heat, Q , are as follows:

$$W = c (d\Delta T/dt) s + \kappa \Delta T$$

$$Q_{i,j} = (W_i + W_j)(t_j - t_i)/(2s), i < j$$

$$Q = \sum Q_{i,j}$$

Experiment 1

$$T = 225.048^\circ\text{C}$$

$$P(\text{O}_2) = 210.2 \text{ kPa}$$

$$m_s = 0.7987 \text{ g}$$

$$\Delta T_{\text{max}} = 0.528^\circ\text{C}$$

$$\kappa = 0.802111 \text{ mW/mm}$$

$$c = 2110.5 \text{ mJ/mm}$$

$$s = 0.015222 \text{ mm/s}$$

$$\theta = 5.933 \times 10^{-3}^\circ\text{C/mm}$$

t (mm)	ΔT (mm)	$d\Delta T/dt$ (mm/mm)	W (mw)	$Q_{i,j}$ (J)	Q (J)
0	0	6.4095	205.9	80.3	80.3
6.4	35.4	4.5920	175.9	68.9	149.1
12.9	60.7	3.0497	146.7	61.3	210.4
20.0	76.1	1.7144	116.1	63.9	274.3
29.7	86.0	0.4799	84.4	44.6	318.9
38.5	89.0	-0.0508	69.8		

Experiment 1 continued

t (mm)	ΔT (mm)	$d\Delta T/dt$ (mm/mm)	W (mw)	$Q_{i,j}$ (J)	Q (J)
53.0	88.0	0.0000	70.6	66.8	385.7
70.6	86.2	-0.4369	55.1	72.7	458.4
96.1	76.4	-0.5926	42.2	81.5	539.9
121.6	62.4	-0.4995	34.0	63.9	603.8
147.0	48.3	-0.3994	25.9	50.0	653.8
172.4	38.0	-0.3199	20.2	38.5	692.2
198.0	30.7	-0.2593	16.3	30.7	722.9
223.2	22.8	-0.2141	11.4	22.9	745.9
248.6	17.5	-0.1791	8.3	16.4	762.3
273.9	12.5	-0.1509	5.1	11.2	773.5
299.3	10.0	-0.1302	3.8	7.5	781.0
324.4	9.2	-0.1130	3.7	6.3	787.2
349.8	7.0	-0.0988	2.4	5.2	792.4
375.1	5.8	-0.0871	1.9	3.6	795.9
400.6	4.5	-0.0773	1.1	2.5	798.4
				1.8	800.2

Experiment 1 continued

t (mm)	ΔT (mm)	$d\Delta T/dt$ (mm/mm)	W (mw)	$Q_{i,j}$ (J)	Q (J)
426.1	4.0	-0.0690	1.0	0.8	801.0
451.5	2.4	-0.0621	-0.1	-0.9	800.1
477.0	1.0	-0.0561	-1.0		

Experiment 2

T = 225.418 °C

 $\kappa = 0.775701$ mW/mmP(O₂) = 211.0 kPa

c = 2248.5 mJ/mm

 $m_s = 0.7985$ g

s = 0.0154235 mm/s

 $\Delta T_{\max} = 0.510$ °C $\theta = 5.473 \times 10^{-3}$ °C/mm

t (mm)	ΔT (mm)	$d\Delta T/dt$ (mm/mm)	W (mw)	$Q_{i,j}$ (J)	Q (J)
0	0	6.6061	229.1	31.8	31.8
2.2	13.3	5.9413	216.4	30.0	61.8
4.4	26.0	5.3111	204.4	51.5	113.2
8.5	46.6	4.2288	182.8	55.9	169.2
13.6	64.2	3.0499	155.6	67.1	236.3
21.1	81.5	1.6534	120.6		

Experiment 2 continued

l (mm)	ΔT (mm)	$d\Delta T/dt$ (mm/mm)	W (mw)	$Q_{i,j}$ (J)	Q (J)
				61.1	297.4
30.2	89.4	0.4981	86.6	36.6	334.0
37.3	93.0	0.0072	72.4	20.2	354.2
41.6	93.2	0.0000	72.3	32.6	386.8
49.1	90.9	-0.2500	61.8	37.6	424.4
59.6	87.0	-0.5482	48.5	54.2	478.6
79.5	74.9	-0.6493	35.6	53.9	532.5
104.9	61.5	-0.5150	29.8	45.4	577.8
130.3	50.0	-0.3900	25.3	38.4	616.3
155.5	41.5	-0.3003	21.8	32.9	649.2
181.1	33.6	-0.2356	17.9	26.1	675.3
206.4	26.4	-0.1895	13.9	20.3	695.6
231.8	20.8	-0.1553	10.7	16.8	712.4
257.2	18.3	-0.1295	9.7	14.6	727.0
282.6	15.2	-0.1095	8.0	11.3	738.3
307.8	11.8	-0.0939	5.9	9.0	747.3
333.1	10.1	-0.0813	5.0	7.8	755.1
358.5	9.0	-0.0710	4.5	6.8	761.9
384.0	7.5	-0.0626	3.6		

Experiment 2 continued

t (mm)	ΔT (mm)	$d\Delta T/dt$ (mm/mm)	W (mw)	$Q_{i,j}$ (J)	Q (J)
435.0	5.7	-0.0496	2.7	10.5	772.4
485.8	3.2	-0.0403	1.1	6.2	778.6
561.9	3.0	-0.0306	1.3	5.8	784.4
638.1	1.0	-0.0240	-0.1	3.0	787.4
650.9	0	-0.0231	-0.8	-0.4	787.1

Experiment 3

$$T = 225.662\text{ }^{\circ}\text{C}$$

$$P(\text{O}_2) = 210.8\text{ kPa}$$

$$m_s = 0.8012\text{ g}$$

$$\Delta T_{\text{max}} = 0.519\text{ }^{\circ}\text{C}$$

$$\kappa = 0.805013\text{ mW/mm}$$

$$c = 2139.7\text{ mJ/mm}$$

$$s = 0.015231\text{ mm/s}$$

$$\theta = 5.544 \times 10^{-3}\text{ }^{\circ}\text{C/mm}$$

t (mm)	ΔT (mm)	d ΔT /dt (mm/mm)	W (mw)	$Q_{i,j}$ (J)	Q (J)
0	0	6.7754	220.8	32.2	32.2
2.3	11.7	6.0343	206.1	24.2	56.4
4.1	29.6	5.4849	202.6	31.8	88.2
6.6	37.1	4.7664	185.2	33.9	122.1
9.5	50.0	3.9980	170.6	41.3	163.4
13.4	64.6	3.0748	152.2	43.6	207.0
18.1	75.6	2.1298	130.3	55.5	262.5
25.3	87.8	1.0397	104.5	54.1	316.6
34.0	93.6	0.2925	84.9	26.8	343.4
39.1	93.6	0.0000	75.3	55.8	399.2
51.7	90.2	-0.3983	59.6	45.3	444.6
64.5	88.6	-0.7078	48.3	69.1	513.7
89.8	69.0	-0.6304	35.0	54.3	568.1
115.1	57.0	-0.4742	30.4		

Experiment 3 continued

\hat{t} (mm)	ΔT (mm)	$d\Delta T/dt$ (mm/mm)	W (mw)	$Q_{i,j}$ (J)	Q (J)
				46.2	614.3
140.4	45.8	-0.3578	25.2	39.2	653.4
166.0	37.7	-0.2753	21.4	33.4	686.8
191.4	32.0	-0.2178	18.7	28.4	715.3
216.7	26.5	-0.1763	15.6	23.4	738.7
242.1	21.4	-0.1453	12.5	34.6	773.3
292.8	14.5	-0.1034	8.3	23.8	797.1
343.7	10.5	-0.0771	5.9	17.3	814.3
394.7	7.9	-0.0597	4.4	11.5	825.8
445.4	5.0	-0.0476	2.5	4.6	830.4
496.1	1.9	-0.0388	0.3	-1.6	828.8
563.1	0	-0.0305	-1.0		

Experiment 4

$$T = 154.993\text{ }^{\circ}\text{C}$$

$$P(\text{O}_2) = 112.1\text{ kPa}$$

$$m_s = 0.8188\text{ g}$$

$$\Delta T_{\max} = 0.037\text{ }^{\circ}\text{C}$$

$$\kappa = 0.058428\text{ mW/mm}$$

$$c = 192.7\text{ mJ/mm}$$

$$v = 0.015212\text{ mm/s}$$

$$\theta = 5.401 \times 10^{-4}\text{ }^{\circ}\text{C/mm}$$

$t\text{ (mm)}$	$\Delta T\text{ (mm)}$	$d\Delta T/dt\text{ (mm/mm)}$	$W\text{ (mw)}$	$Q_{i,j}\text{ (J)}$	$Q\text{ (J)}$
0	0	8.3864	24.6	1.9	1.9
1.7	6.6	3.1061	9.5	1.5	3.4
4.9	13.6	1.4214	5.0	1.1	4.5
8.7	18.5	0.8646	3.6	1.4	5.9
15.2	22.9	0.5177	2.9	1.0	6.9
21.2	25.3	0.2819	2.3	4.2	11.1
46.7	34.2	0.2511	2.7	4.8	15.9
72.0	39.8	0.2228	3.0	10.4	26.3
122.7	47.4	0.1723	3.3	11.4	37.7
173.4	54.3	0.1303	3.6	10.0	47.7
214.2	61.5	0.1026	3.9	16.1	63.7
274.9	67.5	0.0717	4.2	13.6	77.3
325.5	68.5	0.0000	4.0	20.0	97.3
401.7	68.3	-0.0050	4.0		

Experiment 4 continued

t (mm)	ΔT (mm)	$d\Delta T/dt$ (mm/mm)	W (mw)	$Q_{i,j}$ (J)	Q (J)
				19.2	116.5
477.8	64.0	-0.0104	3.7	18.4	134.9
553.8	63.7	-0.0158	3.7	12.1	147.1
604.5	63.0	-0.0288	3.6	11.9	158.9
655.4	62.6	-0.0496	3.5	5.6	164.5
680.8	57.5	-0.0628	3.2	3.9	168.4
706.1	47.2	-0.4357	1.5	3.3	171.7
756.8	22.6	-0.2881	0.5	0.4	172.1
807.7	5.6	-0.1827	-0.2	-0.8	171.2
883.5	1.8	-0.0778	-0.1		

Experiment 5

$$T = 154.925^{\circ}\text{C}$$

$$P(\text{O}_2) = 397.1 \text{ kPa}$$

$$m_s = 0.8262 \text{ g}$$

$$\Delta T_{\text{max}} = 0.064^{\circ}\text{C}$$

$$\kappa = 0.053879 \text{ mW/mm}$$

$$c = 197.2 \text{ mJ/mm}$$

$$s = 0.015184 \text{ mm/s}$$

$$\theta = 5.365 \times 10^{-4}^{\circ}\text{C/mm}$$

$t \text{ (mm)}$	$\Delta T \text{ (mm)}$	$d\Delta T/dt \text{ (mm/mm)}$	$W \text{ (mw)}$	$Q_{i,j} \text{ (J)}$	$Q \text{ (J)}$
0	0	16.7336	50.1	3.9	3.9
1.7	10.5	6.1976	19.1	1.9	5.7
3.5	20.5	3.7186	12.2	3.0	8.7
8.2	33.1	1.8189	7.2	3.3	12.0
16.2	43.5	0.9729	5.3	3.4	15.4
25.7	53.6	0.8600	5.5	5.0	20.4
39.2	65.7	0.7613	5.8	7.0	27.4
56.9	77.9	0.6546	6.2	7.3	34.7
74.6	89.0	0.5533	6.5	7.3	42.1
91.7	96.7	0.4606	6.6	10.1	52.2
114.8	105.0	0.3422	6.7	11.3	63.4
140.2	113.1	0.2249	6.8	10.3	73.7
163.2	118.7	0.1273	6.8	4.8	78.5
174.0	118.7	0.0846	6.6	12.9	91.4

Experiment 5 continued

t (mm)	ΔT (mm)	$d\Delta T/dt$ (mm/mm)	W (mw)	$Q_{i,j}$ (J)	Q (J)
204.2	119.1	-0.0241	6.3	23.8	115.1
267.5	102.2	-0.1500	5.1	21.6	136.7
343.8	77.7	-0.2207	3.5	21.2	157.9
445.1	60.2	-0.1350	2.8	18.2	176.2
546.8	55.3	-0.1254	2.6	14.1	190.3
647.8	35.0	-0.0800	1.6	5.3	195.6
723.9	9.8	-0.0200	0.5	0.9	196.5
782.4	0.0	-0.0080	0		

Experiment 6

$$T = 317.318\text{ }^{\circ}\text{C}$$

$$P(\text{O}_2) = 110.0\text{ kPa}$$

$$\dot{m}_s = 0.8039\text{ g}$$

$$\Delta T_{\max} = 0.616\text{ }^{\circ}\text{C}$$

$$\kappa = 1.207294\text{ mW/mm}$$

$$c = 2404.2\text{ mJ/mm}$$

$$s = 0.061258\text{ mm/s}$$

$$\theta = 5.584 \times 10^{-3}\text{ }^{\circ}\text{C/mm}$$

$t\text{ (mm)}$	$\Delta T\text{ (mm)}$	$d\Delta T/dt\text{ (mm/mm)}$	$W\text{ (mw)}$	$Q_{i,j}\text{ (J)}$	$Q\text{ (J)}$
0	0	16.8860	2486.9	24.1	24.1
0.6	11.3	16.5000	2443.7	23.8	47.9
1.2	24.1	16.2000	2415.0	37.6	85.6
2.2	36.9	14.6102	2196.3	30.4	116.0
3.1	57.1	12.7323	1944.1	74.8	190.8
6.0	79.8	7.5919	1214.5	38.7	229.5
8.4	95.1	4.3887	761.2	41.6	271.1
13.5	107.5	0.7421	239.1	15.5	286.6
18.6	110.3	0.0000	133.2	8.8	295.4
26.1	105.3	-0.7932	10.3	0.5	295.9
36.2	94.4	-0.8000	-3.9	-7.1	288.8
61.5	66.2	-0.7509	-30.7	-7.4	281.4
86.8	47.8	-0.4261	-5.1	1.3	282.7
137.6	29.6	-0.1871	8.2	13.5	296.2
213.8	21.2	-0.0819	13.5		

Experiment 6 continued

t (mm)	ΔT (mm)	$d\Delta T/dt$ (mm/mm)	W (mw)	$Q_{i,j}$ (J)	Q (J)
				25.6	321.8
315.1	19.2	-0.0389	17.4	38.9	360.7
442.1	19.1	-0.0201	20.1	38.4	399.1
568.8	15.6	-0.0123	17.0	38.0	437.2
721.0	12.2	-0.0077	13.6	28.1	465.2
847.8	11.9	-0.0056	13.5	34.2	499.5
999.9	12.1	-0.0040	14.0	34.8	534.3
1152.1	12.0	-0.0030	14.0	28.8	563.1
1279.0	11.7	-0.0025	13.8	32.1	595.2
1431.0	10.3	-0.0022	12.1	29.8	625.0
1583.3	10.1	-0.0020	11.9	24.6	649.7
1710.1	10.1	-0.0020	11.9	27.1	676.8
1847.6	10.3	-0.0010	12.3	24.0	700.8
1967.1	10.3	-0.0008	12.3	23.0	723.8
2091.1	8.7	-0.0005	10.4	37.3	761.2
2369.2	5.0	-0.0001	6.0	22.7	783.9
2673.3	2.6	0.0000	3.1	7.4	791.3
2876.0	1.1	0	1.3	-2.9	788.4
3071.7	-2.6	0	-3.1		

Experiment 7

$$T = 317.476\text{ }^{\circ}\text{C}$$

$$P(\text{O}_2) = 390.9\text{ kPa}$$

$$m_s = 0.7942\text{ g}$$

$$\Delta T_{\max} = 1.060\text{ }^{\circ}\text{C}$$

$$\kappa = 3.86\text{ mW/mm}$$

$$c = 8400\text{ mJ/mm}$$

$$s = 0.061533\text{ mm/s}$$

$$\theta = 1.92 \times 10^{-2}\text{ }^{\circ}\text{C/mm}$$

$$[d\Delta T/dt]_{\max} = 20.3\text{ mm/mm}$$

$$W_{\max} = 10469\text{ mW}$$

Experiment 8

$$T = 174.003\text{ }^{\circ}\text{C}$$

$$P(\text{O}_2) = 329.0\text{ kPa}$$

$$m_s = 0.7935\text{ g}$$

$$\Delta T_{\max} = 0.143\text{ }^{\circ}\text{C}$$

$$\kappa = 0.222350\text{ mW/mm}$$

$$c = 598.6\text{ mJ/mm}$$

$$s = 0.015184\text{ mm/s}$$

$$\theta = 1.978 \times 10^{-3}\text{ }^{\circ}\text{C/mm}$$

$t\text{ (mm)}$	$\Delta T\text{ (mm)}$	$d\Delta T/dt\text{ (mm/mm)}$	$W\text{ (mw)}$	$Q_{i,j}\text{ (J)}$	$Q\text{ (J)}$
0	0	7.7640	70.6	4.7	4.7
1.4	6.8	3.2350	30.9	5.3	10.0
4.9	13.0	1.3159	14.9	4.3	14.2
10.0	18.9	0.7058	10.6	9.9	24.1
22.6	31.9	0.6664	13.1	11.5	35.6
35.3	40.2	0.5873	14.3	14.6	50.1
50.3	48.0	0.4982	15.2	23.7	73.9
73.2	58.0	0.3709	16.3		

Experiment 8 continued

t (mm)	ΔT (mm)	$d\Delta T/dt$ (mm/mm)	W (mw)	$\bar{Q}_{i,j}$ (J)	Q (J)
				24.9	98.8
96.1	65.2	0.2542	16.8	25.4	124.2
119.0	69.7	0.1480	16.8	22.2	146.4
139.2	72.0	0.0632	16.6	13.7	160.1
151.9	72.3	0.0141	16.2	26.9	187.0
177.2	72.1	0.0000	16.0	28.7	215.7
205.2	70.1	-0.0500	15.1	30.7	246.4
238.1	66.5	-0.1788	13.2	41.0	287.4
289.0	57.4	-0.1595	11.3	35.1	322.5
339.8	49.3	-0.1415	9.7	29.2	351.7
390.5	40.3	-0.1249	7.8	34.5	386.2
466.5	31.0	-0.1024	6.0	33.2	419.4
567.9	21.0	-0.0769	4.0	23.4	442.8
669.5	15.9	-0.0566	3.0	17.8	460.6
771.1	12.1	-0.0415	2.3	13.7	474.3
872.2	9.4	-0.0271	1.8	8.8	483.1
973.6	4.9	-0.0271	0.8	3.9	487.0
1049.7	4.0	-0.0200	0.7	1.2	488.2
1108.1	0.0	-0.0100	-0.1		

Experiment 9

$$T = 173.961\text{ }^{\circ}\text{C}$$

$$P(\text{O}_2) = 136.3\text{ kPa}$$

$$m_s = 0.8116\text{ g}$$

$$\Delta T_{\text{max}} = 0.072\text{ }^{\circ}\text{C}$$

$$\kappa = 0.058358\text{ mW/mm}$$

$$c = 151.9\text{ mJ/mm}$$

$$s = 0.015195\text{ mm/s}$$

$$\theta = 5.878 \times 10^{-4}\text{ }^{\circ}\text{C/mm}$$

t (mm)	ΔT (mm)	$d\Delta T/dt$ (mm/mm)	W (mw)	$Q_{i,j}$ (J)	Q (J)
0	0	19.1454	44.2	1.4	1.4
0.6	10.1	11.9658	28.2	2.3	3.7
2.2	20.1	5.9829	15.0	2.4	6.1
5.2	30.2	3.0880	8.9	1.2	7.2
7.3	43.0	2.3067	7.8	3.4	10.6
14.4	55.8	1.5058	6.7	4.1	14.7
23.3	68.3	1.3755	7.2	5.8	20.5
35.3	81.1	1.1879	7.5	5.7	26.2
46.7	94.6	0.9972	7.8	6.7	32.9
59.4	109.5	0.7705	8.2	9.2	42.1
77.0	115.6	0.4312	7.7	7.6	49.7
92.2	121.7	0.1149	7.4	2.4	52.1
97.3	121.9	0.0039	7.1	2.2	54.3
102.3	121.5	-0.2782	6.4	10.6	64.9
127.8	116.5	-0.2858	6.1		

Experiment 9 continued

t (mm)	ΔT (mm)	$d\Delta T/dt$ (mm/mm)	W (mw)	$Q_{i,j}$ (J)	Q (J)
				9.9	74.8
153.2	110.0	-0.2918	5.7	11.7	86.5
186.1	99.0	-0.2971	5.1	26.6	13.2
280.0	72.3	-0.2974	3.5	13.8	127.0
355.8	45.5	-0.2815	2.0	5.5	132.5
406.9	32.3	-0.2627	1.3	3.7	136.2
457.7	25.3	-0.2374	0.9	2.1	138.4
508.5	14.2	-0.2057	0.4	-0.1	138.3
551.0	0	-0.1742	-0.4		

Experiment 10

T = 285.334 °C

P(O₂) = 332.4 kPam_S = 0.7996 g $\Delta T_{\max} = 1.205$ °C $\kappa = 0.989877$ mW/mm

c = 2215.7 mJ/mm

s = 0.061139 mm/s

 $\theta = 5.332 \times 10^{-3}$ °C/mm

t (mm)	ΔT (mm)	d ΔT /dt (mm/mm)	W (mw)	Q _{i,j} (J)	Q (J)
0	0	18.8900	2558.9	138.7	138.7
3.4	21.8	17.7800	2430.2	78.7	217.4
5.5	47.2	15.5400	2151.9	50.6	268.0
7.0	72.5	14.0100	1969.6	43.3	311.3
8.4	97.9	12.6500	1810.5	60.6	371.9
10.6	123.2	10.6100	1559.2	74.6	446.5
13.9	148.5	7.8100	1205.0	66.4	512.9
17.9	174.2	4.8200	825.4	67.0	579.9
25.6	194.1	0.3400	238.2	24.6	604.5
32.0	220.0	0.1000	231.3	46.5	651.0
44.5	226.0	0.0000	223.7	59.4	710.3
62.1	218.0	-0.2000	188.7	51.4	761.7
82.0	186.5	-0.4244	127.1	49.0	810.7
120.0	153.7	-0.8985	30.4		

Experiment 10 continued

t (mm)	ΔT (mm)	$d\Delta T/dt$ (mm/mm)	W (mw)	$Q_{i,j}$ (J)	Q (J)
				23.5	834.2
170.8	117.5	-0.6654	26.2	20.6	854.8
221.5	87.6	-0.4670	23.5	18.0	872.8
272.3	66.4	-0.3386	19.9	15.0	887.8
323.0	51.5	-0.2551	16.4	16.2	904.0
393.0	36.9	-0.1816	11.9	22.2	926.2
518.3	20.3	-0.0764	9.7	26.0	952.3
719.6	10.1	-0.0290	6.1	23.8	976.1
1022.0	5.0	-0.0103	3.6	15.6	991.6
1326.0	3.4	-0.0048	2.7	15.8	1007.4
1730.0	2.4	-0.0022	2.1	10.2	1017.7
2134.0	1.2	-0.0012	1.0	4.1	1021.7
2486.0	0.5	-0.0008	0.4	0.9	1022.6
2839.0	0	-0.0005	-0.1		

Experiment 11

$$T = 285.492\text{ }^{\circ}\text{C}$$

$$P(\text{O}_2) = 136.0\text{ kPa}$$

$$m_s = 0.7993\text{ g}$$

$$\Delta T_{\max} = 0.945\text{ }^{\circ}\text{C}$$

$$\kappa = 0.955697\text{ mW/mm}$$

$$c = 2408.3\text{ mJ/mm}$$

$$s = 0.061270\text{ mm/s}$$

$$\theta = 5.682 \times 10^{-3}\text{ }^{\circ}\text{C/mm}$$

$t\text{ (mm)}$	$\Delta T\text{ (mm)}$	$d\Delta T/dt\text{ (mm/mm)}$	$W\text{ (mw)}$	$Q_i\text{ (J)}$	$Q\text{ (J)}$
0	0	9.7624	1440.5	89.8	89.8
4.1	35.6	8.1923	1242.9	57.6	147.4
7.1	60.6	7.1334	1110.5	65.5	212.9
11.0	86.4	5.8703	948.8	72.2	285.2
16.2	111.5	4.3859	753.7	78.0	363.2
23.7	137.0	2.6468	521.5	61.4	424.6
32.6	153.3	1.1989	323.4	45.1	469.7
43.0	163.0	0.3539	208.0	37.4	507.0
55.5	165.5	0.0000	158.2	31.3	538.3
68.3	163.5	-0.1000	141.5	24.6	563.0
81.0	158.0	-0.3225	96.0	24.1	587.1
106.2	142.0	-0.7762	21.2	6.9	593.9
131.5	125.7	-0.7320	12.1	5.5	599.4
156.8	111.1	-0.6223	14.4	13.9	613.4
212.8	81.4	-0.4177	16.2		

Experiment 11 continued

t (mm)	ΔT (mm)	$d\Delta T/dt$ (mm/mm)	W (mw)	$Q_{i,j}$ (J)	Q (J)
				23.4	636.8
309.2	49.9	-0.0309	13.6	17.9	654.7
410.9	30.1	-0.0409	8.0	8.3	663.0
498.5	19.1	-0.0995	3.6	13.4	676.3
757.6	7.5	-0.0300	2.7	13.0	689.3
1063.8	3.7	-0.0074	2.5	11.4	700.7
1370.5	2.9	-0.0044	2.1	9.0	709.7
1677.1	2.0	-0.0030	1.5	2.9	712.6
1983.5	0.0	-0.0021	-0.3		

Experiment 4a

$$T = 154.923\text{ }^{\circ}\text{C}$$

$$P(\text{O}_2) = 210.8\text{ kPa}$$

$$m_s = 0.7973\text{ g}$$

$$\Delta T_{\text{max}} = 0.044\text{ }^{\circ}\text{C}$$

$$\kappa = 0.087112\text{ mW/mm}$$

$$c = 268.8\text{ mJ/mm}$$

$$s = 0.015238\text{ mm/s}$$

$$\theta = 6.268 \times 10^{-4}\text{ }^{\circ}\text{C/mm}$$

t (mm)	ΔT (mm)	$d\Delta T/dt$ (mm/mm)	W (mw)	$Q_{i,j}$ (J)	Q (J)
0	0	8.3438	34.2	3.1	3.1
1.8	11.4	4.2160	18.3	2.8	5.9
4.2	21.4	3.7293	17.1	3.2	9.1
7.2	31.8	3.1641	15.7	3.6	12.7
10.9	41.6	2.5333	14.0	4.1	16.8
15.7	52.0	1.8238	12.0	4.6	21.4
22.1	62.1	1.0694	9.8	6.5	27.9
34.0	68.4	0.2481	7.0	4.5	32.5
44.1	70.2	0.1446	6.7	10.4	42.9
68.9	65.7	0.0806	6.1	19.6	62.5
119.7	63.0	0.0576	5.7	34.7	97.2
210.0	67.8	0.0191	6.0	33.8	131.0
297.0	68.0	-0.0152	5.9	30.3	161.3
378.1	65.5	-0.0448	5.5	24.9	186.2

Experiment 4a continued

t (mm)	ΔT (mm)	$d\Delta T/dt$ (mm/mm)	W (mw)	$Q_{i,j}$ (J)	Q (J)
449.6	61.5	-0.0689	5.1	30.8	216.9
550.7	52.9	-0.0998	4.2	24.2	241.2
652.1	41.4	-0.1271	3.1	13.0	254.1
728.2	31.0	-0.1452	2.1	8.4	262.6
804.3	19.3	-0.1000	1.3	4.1	266.7
880.7	6.5	-0.0500	0.4	0.9	267.6
956.4	0.0	0.0000	0.0		

Experiment 5a

 $T = 173.948\text{ }^{\circ}\text{C}$ $P(\text{O}_2) = 211.4\text{ kPa}$ $m_s = 0.8322\text{ g}$ $\Delta T_{\text{max}} = 0.111\text{ }^{\circ}\text{C}$ $\kappa = 0.062248\text{ mW/mm}$ $c = 173.6\text{ mJ/mm}$ $s = 0.015188\text{ mm/s}$ $\theta = 5.704 \times 10^{-4}\text{ }^{\circ}\text{C/mm}$

$t\text{ (mm)}$	$\Delta T\text{ (mm)}$	$d\Delta T/dt\text{ (mm/mm)}$	$W\text{ (mw)}$	$Q_{i,j}\text{ (J)}$	$Q\text{ (J)}$
0	0	23.7158	62.5	3.6	3.6
1.2	13.2	10.7791	29.2	3.8	7.4
3.8	29.8	4.9408	14.9	1.4	8.8
5.4	41.4	3.7056	12.3	2.7	11.5
9.1	53.8	2.3481	9.5	3.4	14.9
14.1	66.9	2.5376	10.9	1.8	16.7
16.6	75.0	2.4419	11.1	3.6	20.3
21.5	87.7	2.2601	11.4	3.9	24.2
26.6	99.9	2.0791	11.7	6.1	30.3
34.4	114.8	1.8187	11.9	6.1	36.4
42.1	128.5	1.5811	12.2	10.2	46.6
54.8	144.8	1.2311	12.3	10.1	56.7
67.3	157.3	0.9377	12.3	10.3	66.9
80.0	167.7	0.6917	12.3	10.2	77.1

Experiment 5a continued

t (mm)	ΔT (mm)	$d\Delta T/dt$ (mm/mm)	W (mw)	$Q_{i,j}$ (J)	Q (J)
92.6	176.2	0.4993	12.3	16.5	93.6
113.0	184.8	0.2970	12.3	20.3	113.9
137.8	191.2	0.2331	12.5	12.8	126.7
153.5	193.6	0.1000	12.3	37.7	164.4
204.3	190.7	-0.6125	10.3	31.9	196.3
255.0	164.4	-0.5222	8.9	25.9	222.3
305.7	126.1	-0.4421	6.7	21.8	244.1
356.4	118.6	-0.3728	6.4	20.4	264.5
407.3	105.5	-0.3118	5.7	17.1	281.6
457.9	83.5	-0.2621	4.5	19.7	301.3
533.9	62.9	-0.2062	3.4	16.2	317.5
610.1	57.0	-0.1730	3.1	12.1	329.6
787.7	23.6	-0.1400	1.1	2.8	341.8
838.4	14.1	-0.1250	0.5	0.4	342.2
889.0	0.0	-0.1100	-0.3		

Experiment 10a

$$T_i = 285.615\text{ }^{\circ}\text{C}$$

$$P(\text{O}_2) = 210.4\text{ kPa}$$

$$m_s = 0.7968\text{ g}$$

$$\Delta T_{\text{max}} = 1.080\text{ }^{\circ}\text{C}$$

$$\kappa = 0.981214\text{ mW/mm}$$

$$c = 2426.6\text{ mJ/mm}$$

$$s = 0.061119\text{ mm/s}$$

$$\theta = 5.699 \times 10^{-3}\text{ }^{\circ}\text{C/mm}$$

t (mm)	ΔT (mm)	$d\Delta T/dt$ (mm/mm)	W (mw)	$Q_{i,j}$ (J)	Q (J)
0	0	12.6550	1876.9	84.0	84.0
2.9	12.7	11.1275	1662.8	60.0	143.9
5.2	43.2	9.9867	1523.5	50.3	194.2
7.3	68.5	8.9997	1402.0	58.6	252.8
10.0	93.9	7.8073	1250.0	64.5	317.3
13.4	119.3	6.4282	1070.4	73.7	391.0
18.1	144.7	4.7468	846.0	99.2	490.2
27.1	169.9	2.2557	501.2	66.2	552.4
36.9	184.5	0.6316	274.7	48.6	601.0
49.8	189.5	0.0000	185.9	30.1	631.1
62.5	181.4	-0.5000	103.8	32.8	663.9
87.8	170.8	-0.7607	54.8	37.5	701.4
138.3	134.9	-0.6500	36.0	24.4	725.8
189.1	103.6	-0.5326	22.7		

Experiment 10a continued

t (mm)	ΔT (mm)	$d\Delta T/dt$ (mm/mm)	W (mw)	$Q_{i,j}$ (J)	Q (J)
				28.3	754.1
265.3	71.1	-0.3172	22.7	29.1	783.2
366.8	40.2	-0.1827	12.3	13.4	796.6
445.8	28.1	-0.1289	8.4	10.6	807.2
535.6	20.0	-0.0922	6.0	7.7	815.0
637.9	13.4	-0.0666	3.3	8.0	822.9
841.6	7.5	-0.0394	1.5	11.0	834.0
1268.3	4.7	-0.0200	1.6	12.8	846.8
1655.3	3.8	-0.0090	2.4	15.5	862.3
2062.8	2.9	-0.0040	2.3	10.6	872.8
2571.7	0.6	-0.0020	0.3	0.7	873.6
2876.9	0.0	0.0000	0.0		

Experiment 6a

$$T = 317.467\text{ }^{\circ}\text{C}$$

$$P(\text{O}_2) = 209.4\text{ kPa}$$

$$m_s = 0.8119\text{ g}$$

$$\Delta T_{\text{max}} = 0.941\text{ }^{\circ}\text{C}$$

$$\kappa = 1.157773\text{ mW/mm}$$

$$c = 2505.0\text{ mJ/mm}$$

$$s = 0.061295\text{ mm/s}$$

$$\theta = 5.791 \times 10^{-3}\text{ }^{\circ}\text{C/mm}$$

t (mm)	ΔT (mm)	$d\Delta T/dt$ (mm/mm)	W (mw)	$Q_{i,j}$ (J)	Q (J)
0	0	34.3380	5272.4	91.1	91.1
1.2	34.6	26.0000	4032.2	35.1	126.2
1.8	60.0	20.0000	3140.4	33.9	160.1
2.5	85.5	17.5357	2791.5	61.5	221.6
4.0	110.7	13.7377	2237.5	67.7	289.3
6.2	136.2	8.9783	1536.3	76.8	366.1
10.8	156.3	2.1432	510.0	29.7	395.8
15.8	162.1	0.2000	218.4	17.2	413.0
21.4	162.9	-0.2000	157.9	21.2	434.2
30.2	158.8	-0.3000	137.8	68.7	502.9
66.6	131.6	-0.3826	93.6	75.1	578.0
142.6	87.4	-0.4798	27.5	47.0	625.0
243.8	53.7	-0.2135	29.4	33.9	658.9
320.1	39.4	-0.1334	25.1		

Experiment 6a continued

t (mm)	ΔT (mm)	$d\Delta T/dt$ (mm/mm)	W (mw)	$Q_{i,j}$ (J)	Q (J)
401.2	30.5	-0.0889	21.7	31.0	689.9
527.8	19.9	-0.0535	14.8	37.7	727.6
679.9	15.1	-0.0332	12.4	33.8	761.3
832.3	12.0	-0.0225	10.4	28.4	789.7
984.2	12.1	-0.0163	11.5	27.2	816.9
1136.4	10.2	-0.0123	9.9	26.6	843.5
1339.0	9.6	-0.0090	9.7	32.5	876.0
1465.7	4.8	-0.0075	4.4	14.6	890.6
1592.2	2.3	-0.0064	1.7	6.3	896.9
1719.1	1.2	-0.0055	0.5	2.3	899.2
1795.3	0.0	-0.0050	-0.8	-0.1	899.0